Phases of He^3 and He^4 Monolayer Films Adsorbed on Basal-Plane Oriented Graphite*

M. Bretz,† J. G. Dash, D. C. Hickernell,‡ E. O. McLean,§ and O. E. Vilches
Department of Physics, University of Washington, Seattle, Washington 98195
(Received 2 January 1973)

Heat capacities of He^3 and He^4 monolayers adsorbed on "Grafoil" graphite substrates at low temperatures are qualitatively different from previous results using other adsorbents. The present study consists of a detailed survey of many samples conducted in two similar but independent calorimeters: the fractional coverages ranged from 5 to 115% of a completed first layer and the temperature range extended from 0.04 to above 10° K. Several distinct thermodynamic regimes are seen, some of which correspond closely with well-known theoretical models as well as others that had not been predicted. At moderate densities and temperatures the behavior resembles that of two-dimensional gases. Departures from ideality are correlated with quantum-mechanical virial corrections for interacting molecules. In this range of coverages the He^4 specific heats begin to rise at $T \gtrsim 3°K$, forming strong rounded peaks near 1°K. He^3, on the other hand, shows a monotonic decrease with falling temperature until $T \simeq 0.2°K$, then (for a narrow range of coverages) reversing the trend to form rounded maxima near 100 m°K. At the lowest temperatures the He^3 appears to enter a two-dimensional ($2D$) Fermi-liquid regime. At higher coverage both He^3 and He^4 undergo second-order phase transitions to regular arrays in registry with the substrate. In the critical region that heat capacities have symmetric peaks of logarithmic shape, with coefficients in close quantitative agreement with exact $2D$ Ising models. Above critical density the ordering peaks disappear and $2D$ liquid and solid behavior is seen. He^4 at high density and low T is Debye-like, with characteristic temperatures Θ_{2D} equal to Θ_{3D} of hcp solid He^4 of the same interatomic spacing. At higher T the $2D$ solid appears to transform to a $2D$ fluid by a continuous process, and pronounced heat-capacity peaks associated with the transformation are located at temperatures near the melting points of hcp He^4 having the same interatomic spacing. At very low coverage the $2D$ gas character gives way to a regime resembling a low-density $2D$ solid.

I. INTRODUCTION

This paper is a full report of experimental studies which have been described in several recent letters[1–4] and theses.[5,6] The work is part of a continuing program of research on adsorbed films at the University of Washington, but the present results are in sharp qualitative disagreement with previous measurements on other substrates. We believe that the new observations indicate that the present adsorption systems are much closer approximations to the uniform ideal than has been typical of work on helium films. In this introduction we survey relevant portions of the history of experimental and theoretical studies on physical adsorption of helium and other gases, leading up to the present study.

A. Previous Studies of Helium Monolayers

Previous measurements of the heat capacity of adsorbed He films were made with substrates of jeweller's rouge,[7] porous Vycor glass,[8] N_2-plated Vycor,[9] and Ar-plated sintered copper.[10] At densities near full monolayer coverage these films have heat capacities resembling two-dimensional (2D) solids. The characteristic temperatures for all of these films are in the range 20–30°K. This consistency was taken as evidence that the measurements referred to intrinsic properties of the He films, i.e., that the substrates were simply acting as uniform adsorbing planes. But an extensive study of He^3 and He^4 on Ar-plated Cu[11] down to low coverages suggested that the substrates were playing more active roles: Those experiments showed that the 2D solidlike properties persisted even at 0.1 monolayer and 4.2°K, although it had been expected that at such low coverages and high temperatures the film would resemble a 2D gas. The persistence of the "solid" was judged to indicate clustering, with a large latent heat of lateral evaporation. The lower limit of lateral binding was estimated to be an order of magnitude greater than theoretical estimates for mobile 2D He^3[12] and He^4.[13,14] A possible contribution to lateral binding due to substrate phonon exchange[15] was predicted to be comparable to the bare atomic interaction, but still too small to account for the results. A series of experiments[16] specifically designed to detect variations in film properties caused by preplating with one or two layers of Ne or Ar gave a null result: It was then concluded that the nature of the immediate adsorbing surface could not be the determining factor. Nevertheless, the need to invoke substrate properties was emphasized by another series of experiments[17] in which the heat capacity of He^4 was measured at still lower coverages and higher temperatures than heretofore: The new limit for

the apparent lateral heat of vaporization was at least 60°K. This large value could only mean that the substrates, rather than merely enhancing the intrinsic He attractions, must be the prime actors in the experimental systems. Recent measurements by Daunt and co-workers, of the heat capacities of helium on bare and rare-gas-plated Cu[18] are consistent with the above indications.[19]

A possible mechanism for the substrate contribution was proposed by Roy and Halsey,[20] in terms of adsorption heterogeneities. Nonuniformity in adsorption is known to be characteristic of all but a very few adsorbents.[21] Vapor-pressure isotherms and isosteres of typical adsorbent-adsorbate systems indicate that the binding energies of adsorption have relatively wide variations. It is conventionally assumed that these variations take the form of random spatial distributions of localized adsorption sites with differing binding energies. Roy and Halsey proposed a different model, suggesting that the heterogeneities of the substrates in the helium studies were spatially correlated, so that the binding energy would have a relatively long-range variation along the surface. Long-range variations would tend to force adsorbed atoms into dense clusters on the more strongly attractive regions. Such clusters might have heat capacities similar to 2D solids due to their high areal densities, but to distinguish them from the ideal 2D model, Roy and Halsey proposed that they be termed pseudo-Debye. The Roy and Halsey theory does not treat all of the questions arising from the several experiments, but it is extremely appealing in that it answers the major puzzle—the abnormal persistence of 2D solidlike behavior to low densities and high temperatures—by an argument based on the properties of real adsorbents. The essential correctness of their model seems to be borne out by the present experiments, on the basis of two quite different sets of evidence: (a) the several correspondences between the present films on graphite and plausible theoretical models, and (b) the independent evidence for the greater homogeneity of graphite substrates. The main body of this paper has to do with (a). Although (b) involves the published work of other investigators, we give a brief outline of those principal features which are relevant to the present study.

B. Uniform and Heterogeneous Substrates

There is voluminous literature dealing with physical adsorption.[21] On the basis of the many adsorbate-adsorbent combinations that have been examined experimentally, one is forced to the conclusion that heterogeneity is the rule: Regardless of the care in preparing any arbitrary surface, it should be assumed to be nonuniform unless proven otherwise. A second and equally important conclusion, although inferred more from reasoning than from direct evidence, is that uniformity can be judged only within the context of specific physical properties: What may seem to be a uniform system with regard to a certain type of measurement may be quite heterogeneous to another.

A small number of substrates has been found to be exceptionally uniform to physisorption. The prototype of uniform substrates is graphitized carbon black. Attention was drawn to this material by the work of Polley, Schaeffer, and Smith,[22] who discovered that carbon black which had been subjected to high-temperature heat treatment displayed stepwise vapor-pressure isotherms in argon adsorption. The stepwise isotherms were taken as evidence of distinct layer formation, approaching the ideal forms predicted by Fowler and Guggenheim,[23] Hill,[24] and Halsey.[25] Carbon blacks which had been subjected to higher temperatures yielded more distinct steps, and this evidence of increasing homogeneity can be correlated with x-ray[26] and electron-microscopy[27] indications of progressive graphitization, which produces basal-plane structure on all of the exposed surfaces of the particles.[27] The purity of crystal-plane exposure is essential, since the binding energies and presumably other physical properties of films on different facets of the same crystal can be significantly different.[28–30]

A series of studies of argon and krypton adsorption on graphitized carbon black at liquid-N_2 temperature was carried out by Singleton and Halsey.[31] They found that the steps in the Kr isotherms are significantly sharper: This is attributed to the Kr being at a lower effective temperature, relative to the adatom-substrate interaction, than argon. Stepwise isotherms have only been obtained with a relatively small number of carefully prepared substrates. The stepped shape is qualitatively different from the familiar sigmoid curve of the Brunauer-Emmett-Teller (BET) isotherm.[32] Although the BET equation is derived from a simple model, it is now realized that the model is quite unphysical. The sigmoid shape is usually a result of the superposition of stepwise isotherms, but will also occur in uniform systems at temperatures which are comparable to, or larger than, the differences in binding energy of the individual layers.

A material related to graphitized carbon black—exfoliated graphite—has been found to give even sharper steps in the vapor-pressure isotherms. Exfoliation involves the formation of intercalation complexes within layer-structured crystals and subsequent heating which explodes the layers

apart.[33] The discovery of exfoliated graphite as a particularly uniform substrate and its subsequent use for vapor-pressure studies has been described in a series of papers by Thomy and Duval.[34,35] They attribute the apparent superiority of exfoliated graphite over graphitized carbon black to the larger areas of the individual adsorption surfaces, postulating that the small grain size (~0.2 μ) of graphitized carbon black produces some capillary condensation. The reasons for the improvement are not certain, but the evidence is convincing. Features in the vapor-pressure isotherms of methane, Ne, Ar, Kr, and Xe indicate a succession of phase changes in the first monolayer. Thomy and Duval saw no evidence of such structure in films on graphitized carbon black: Its absence may be due to heterogeneity, although temperature nonuniformity might be responsible. A small variation of temperature and/or substrate binding energy could completely obscure any evidence of phase changes, while causing only a slight degree of rounding of the stepwise isotherms. Thus, the graphitized carbon black adsorbent might be quite homogeneous with respect to layer formation, yet strongly heterogeneous with respect to the properties of each individual layer.

II. EXPERIMENTAL DESIGN

Concurrent with the accumulation of the evidence described in Sec. I, it was decided to start a new series of specific-heat measurements of helium films using substrates of expanded graphite. Before reaching the experimental state, a suitable calorimeter cell had to be constructed and characterized. This section describes the two cells (A and B) and the cryostats in which they were used, and adsorption isotherms taken to determine their Ar, He^3, and He^4 monolayer capacities.

A. Substrates, Cells, and Cryostats

The substrate used in all the measurements is a commercially available form of expanded graphite, GTA grade Grafoil.[36] This product is apparently manufactured from natural Madagascar graphite crystals by a mechanical process which produces a marked increase in the total area of basal-plane surfaces available for gas adsorption, and then rolled into sheets of various densities and thicknesses.[37] We now believe that an earlier description[1] of Grafoil as chemically exfoliated pyrolytic graphite is incorrect. The Grafoil sheets used in our studies have densities on the order of one-half that of crystalline graphite. Chemical analysis of a typical sample indicates impurity levels of 10-ppm Si, 1-ppm Mn, 10-ppm Fe, and 1-ppm Cu.[38] The manufacturer's quotation of typical impurity levels is somewhat higher: 40-ppm Al, 30-ppm Mn, 20-ppm Fe, 80-ppm Si, with a total ash residue of 0.1%. The impurities are mainly in the form of inclusions which are present in the initial crystals.[37] X-ray diffraction[39] indicates good alignment of the basal planes parallel to the Grafoil sheet surface, with a mean spread of about 7°. Interlayer spacing corresponds closely to that of natural rather than pyrolytic graphite. There is appreciable broadening of the diffraction lines. If the broadening is attributed to the finite thickness of crystalline laminae in the sheet, their mean thickness is ~100 planes. With this value and the measured density we estimate that the mean separation between laminae normal to the planes is several hundred Å. Through the thickness of a 0.04-cm-thick Grafoil sheet there are approximately 6000 basal-plane surfaces exposed for adsorption. The estimate of surface area based upon the line-broadening measurement agrees closely with the value 20 m^2/g obtained from adsorption. Optical microscopy shows that the lateral dimensions of the optically uniform regions are typically 3 μ.[40] Scanning electron microscopy has not yielded any useful information.

Graphite is a poor and anisotropic thermal conductor at helium temperatures, and so the following elaborate procedure was used to construct cell A. Since cell A performed well in heat-capacity measurements, an almost identical procedure was followed in the construction of cell B, intended for very-low-temperature measurements. Physi-

TABLE I. Physical characteristics of heat-capacity cells.

	Grafoil sheet thickness (cm)	Density of Grafoil (g/cm^3)	Mass of copper container (g)	Mass of Grafoil in cell (g)	Total mass of cell[a] (g)
Cell A	0.040	0.74	13.3	10.9	28.16
Cell B	0.0254	1.1	17.5	11.3	31.5

[a]The difference between the sum of columns 3 and 4 and column 5 is due to the copper powder and solder used in the cells.

cal characteristics of both cells are given in Table I.

Parallel lines about 1.3 mm apart and 0.2–0.3 mm deep were scribed with a scalpel on each surface of the Grafoil sheet. For rigidity, lines on one surface were perpendicular to those on the other surface. The scribed sheets were then heated in vacuum to 750–800°C for several hours, and purged many times with pure helium gas. Disks having a diameter of $\frac{5}{8}$ in. (cell B) were punched from the sheet, placed in a vacuum evaporator, and a 0.5-μ-thick copper film was deposited on their surfaces.

A very thin-walled copper capsule was constructed to house the Grafoil disks. These were lightly pressed into it, with a small amount of cleaned fine-copper powder sprinkled between the disks. By scaling previous measurements[11] on this same grade of copper powder, we estimate that the effective adsorption area due to copper in the present graphite cells amounted to approximately 0.8% of the total. A $\frac{1}{8}$-in. hole was drilled through the center of the Grafoil disks of cell A, while four $\frac{1}{16}$-in. holes were drilled in cell B. These holes were intended for accelerating the equilibrium times for adsorption of each experimental gas sample, so that the film density would be uniform throughout the calorimeter. A lid was temporarily fitted to the capsule to prevent further exfoliation and the assembly heated in vacuum to about 1000°C, left there several hours, then flushed with helium gas. Cell A was cooled in vacuum and then filled with Ar gas, while cell B was cooled in a helium atmosphere. This heat treatment sintered together the Grafoil disks, the copper powder, and the copper container. The lid was attached to the cell by silver soldering in a vacuum furnace at 800°C. Cell A was again allowed to cool in vacuum, then filled with Ar gas, while cell B was soldered in H_2 atmosphere, then cooled in He atmosphere. All succeeding manipulations of both cells were done in a helium atmosphere. Physical characteristics of the cells are listed in Table I.

Cell A was fitted with a $\frac{1}{64}$-in.-o.d. stainless-steel capillary tube, while cell B had a $\frac{1}{64}$-in.-o.d. Cu-Ni tube and a 0.083-in.-o.d. copper tube soft soldered to it. During heat-capacity measurements both cells were connected to external gas-handling systems via the capillary. The larger tube of cell B was used for the isotherm work on this cell. Cell A was mounted in an adiabatic demagnetization cryostat for use above 0.4°K, while cell B was installed in a dilution refrigerator. The cell could be cooled to about 35 m°K by using a superconducting heat switch, but its thermal isolation was poor above 2°K, giving increased point scatter. Diagrams for the two experimental

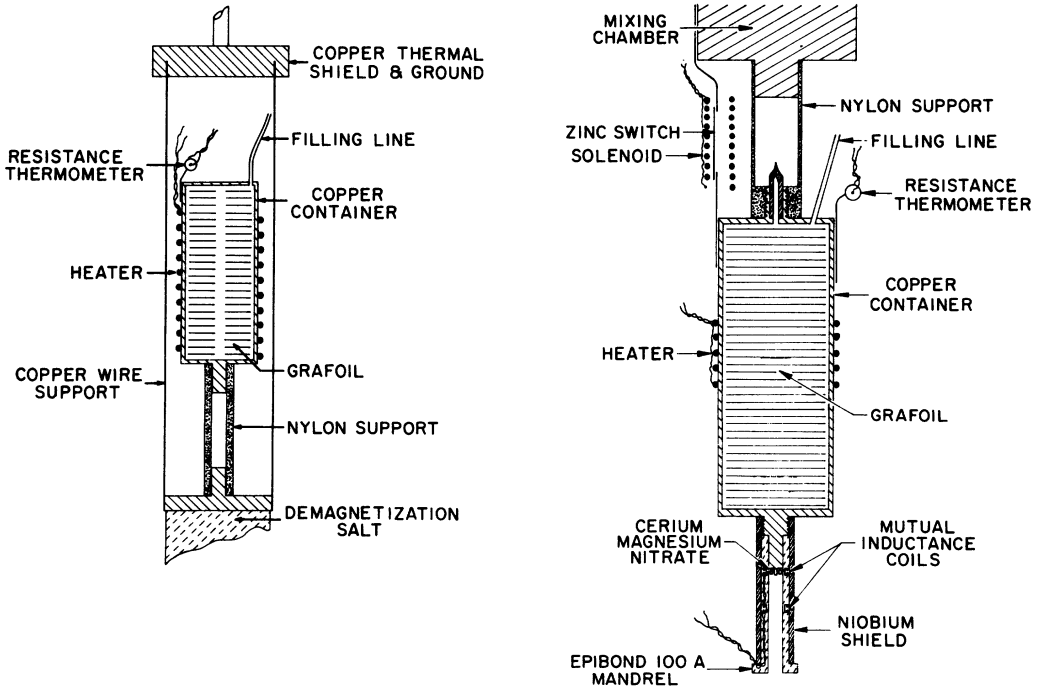

FIG. 1. Experimental cell arrangements in system A (left) and system B (right).

arrangements are shown in Fig. 1.

Heat-capacity measurements were done by the conventional method of introducing a known amount of heat and measuring the resulting change in temperature. The temperature drift of the cell was followed before and after the heat pulse, and the measured drifts were extrapolated to the center of the heating interval.

Heat was applied with an Evanohm wire electric heater (cell A ≡ 424 Ω, cell B ≡ 104 Ω) glued to the cell with GE 7031 varnish. Temperature and temperature changes were measured for cell A with Allen-Bradley 56-Ω and Speer 100-Ω carbon-resistance thermometers which were attached to the cell with a mixture of Apiezon N grease and copper powder. They were calibrated against the vapor pressure of liquid He^4. Temperatures of cell B were measured with a 56-Ω Allen-Bradley resistor above 0.9°K; at lower temperatures we used the susceptibility of 5.6 mg of cerium magnesium nitrate (CMN). Both were calibrated against a Cryo Cal[41] germanium resistor between 1.5 and 4.2°K. During heat-capacity measurements the CMN was checked against the resistor at the end of every set of measurements (usually at least once a day). The susceptibility of the CMN was measured using a superconducting magnetometer.[42] This system provided adequate sensitivity, but the occasional skipping of a flux quantum made necessary the periodic calibration check.

The heat-capacity data presented in Sec. III were obtained in the following way. The heat capacity of the "empty" calorimeter (without helium) was measured over the entire temperature range (and checked several times over the course of the study). A polynomial was fitted to the measured points, and the coefficients of the polynomial were included in a computer program for reducing the raw data.

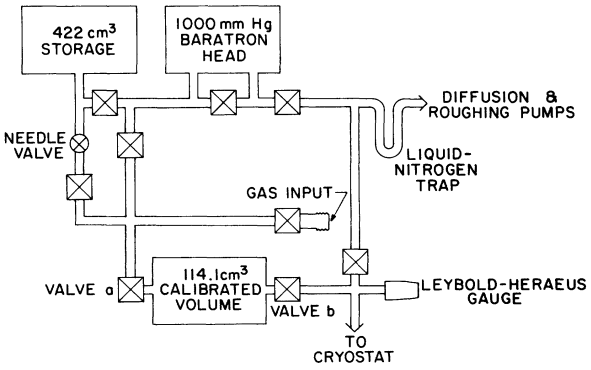

FIG. 2. Schematic diagram of the system B gas-handling system.

Then a gas sample was prepared. Figure 2 shows the gas-handling system used for cell B. A similar system was used for cell A. With valve "*b*" closed, gas from the storage tank was admitted to the calibrated volume and its pressure was measured with a Baratron capacitance gauge.[43] The temperature of the gas was recorded. Then valve "*a*" was closed and valve "*b*" opened into the cryostat.

Gas was introduced to the cell incrementally. For large increments the temperature of the cell increased dramatically, well above 10°K. For small increments, as when slightly changing the coverage to survey a specific film feature, we intentionally warmed the cell to at least 7 or 8°K, to assure uniform density. The cell was then left for several hours, usually overnight. A Leybold pressure gauge measured the room-temperature residual pressure. For submonolayer coverages this pressure was never more than a few microns after the gas had been adsorbed. Since a monolayer is of the order of 100 cm^3 STP of gas (see Table II), the amount of gas left in the calibrated volume was very small. The filling procedure for capsule A differed in that the capsule was filled and isolated at relatively high manifold pressure, allowing a more rapid film equilibrium. Upon warmup, the exhausted gas was measured as a check against possible filling errors.

The heat capacity of sample plus calorimeter was measured and the heat capacity of the film was obtained by subtracting the interpolated background from the measured total.

Annealing of the samples above 4°K appears to be important. Measurements of the lattice gas-ordering peaks (see Sec. III C) of He^4 showed that rapid cooling of a sample after the gas was introduced to the cell resulted in truncated peaks, such as might be due to a distribution of several possible configurations.

B. Adsorption Isotherms

The He^3 and He^4 monolayer capacities of both cells were measured at 4.2°K and the Ar capacities at 77°K. Known amounts of gas were admitted to the cells from a calibrated volume and the gas

TABLE II. Monolayer capacities (cm^3 STP).

	Argon isotherm at 77 °K		Helium-4 isotherm at 4.2 °K		Helium-3 isotherm	
	BET [a]	Point B [a]	Point A	Point B [a]	Point A	Point B
Cell A	68 [b]	···	98	100	92	95
Cell B	83	81	113	116	109	111

[a] For an explanation of the meaning of BET, point A, and point B, see text.
[b] All volumes quoted are uncertain to ±2 cm^3 STP.

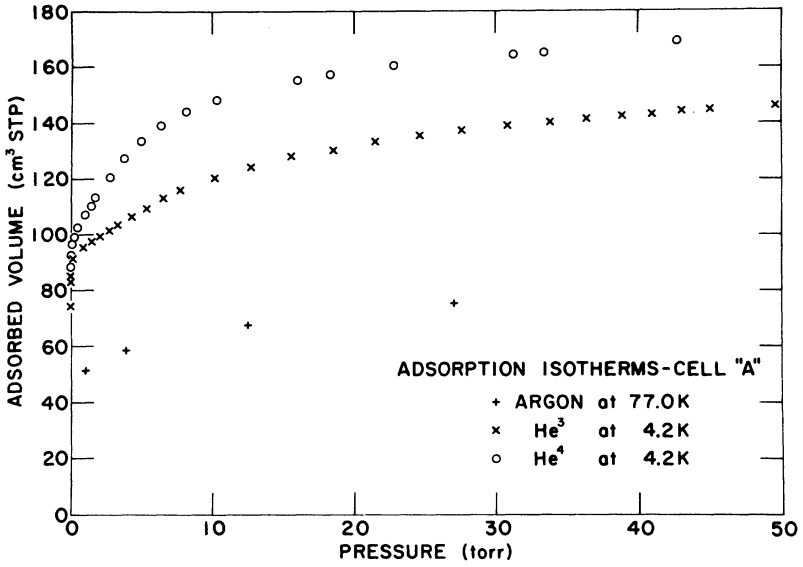

FIG. 3. Examples of vapor-pressure isotherms obtained in system A.

pressure was recorded after sufficient time had elapsed for the cell to reach internal equilibrium. Pressures were measured at room temperature with a Baratron[43] gauge. Thermomolecular pressure corrections for both helium isotopes[44] were made to the A data for pressures lower than 4 Torr, while corrections were made to B data below 2 Torr.

Results are plotted in Figs. 3 and 4. Monolayer capacities N_m computed from these curves using different fiducial points[32] are indicated in Table II. The Ar isotherm follows the BET equation, but since no simple isotherm model fits the He data, points A and B have been chosen in the following way. Henry's law[21] predicts that for low pressures and low coverages the amount of adsorbed gas will be proportional to the gas pressure if the substrate is uniform. In our case we believe that the small linear region at low pressures near the vertical axis is due to the Henry's-law behavior at low coverages of the second layer. Extrapolation of this linear region to $P=0$ defines point A, while the approximate point of departure of the low-pressure experimental points from this line is point B. For comparison, the He^4 monolayer capacity obtained from heat-capacity measurements in cell A is approximately 96.5 cm^3. (See Sec. III D 2.)

In this paper we depart from the conventional

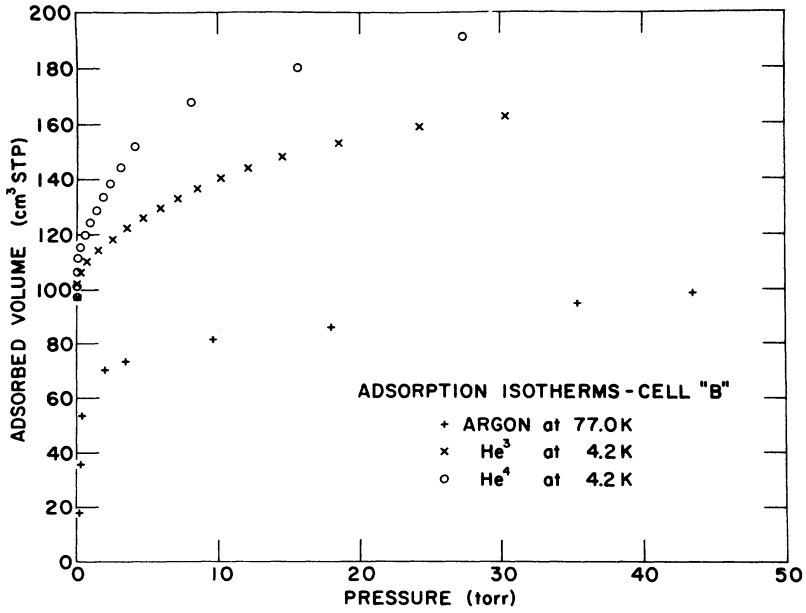

FIG. 4. Examples of vapor-pressure isotherms obtained in system B.

specification of film density as the fractional monolayer coverage N/N_m, where N_m is the number of atoms in a "completed" first monolayer. The location of N_m from vapor-pressure isotherms is imprecise and there is no standard convention leading to a well-defined reference point or criterion of completion. The density of a completed first layer is not a fixed quantity, since it has a small but perceptible temperature dependence. A much more precise fiducial quantity for the He-graphite system is the critical number N_c of He^4 atoms for the lattice-gas ordering transition at $T \simeq 3°K$. As described in Sec. III C the sensitivity to N of the ordering-transition heat-capacity peaks permits specification of N_c to within 1%, and all other coverages can be scaled to this value. Furthermore, the identification of the structure of the ordered He^4 film leads to a substrate area calibration of comparable precision, thereby permitting all films (including those of other adsorbates) to be specified in terms of the areal density $n \equiv N/A$. With this method we find that the density of a full He^4 monolayer at $T = 1°K$ (see Sec. III D 2) is $n_m = 0.115$ Å^{-2}.

There have been three independent studies of He^4 adsorption on Grafoil substrates. Daunt and Lerner[45] and Stewart, Siegel, and Goodstein[46] obtained 4.2°K vapor-pressure isotherms closely resembling ours in shape. Although they used different methods for determining their adsorption areas, both studies yielded estimates within a few percent of ours. Elgin and Goodstein[47] have carried out some heat-capacity measurements of He^4 on Grafoil, at submonolayer coverages and at temperatures between 1 and 4°K. They have also made extensive vapor-pressure measurements at elevated temperatures, down to very low coverages. (See *Note added in proof.*)

III. EXPERIMENTAL RESULTS

The specific-heat behavior indicates several distinctive regimes, shown in the phase diagram of Fig. 5. Several of these regimes have been described briefly in previous communications[1–4]: Here we present more complete descriptions of the results and their analysis, including some features not reported earlier. In most of the subsequent graphs we show only representative data points for purposes of economy and clarity of presentation.[48]

A. 2*D* Gases: Pseudoclassical Regime

1. *General Features*

The heat capacity of an ideal 2D classical gas is $C = Nk$. If we identify as 2D gases all regions having temperature-independent heat capacities and with values falling within about ±10% limits of Nk, the gas regime is seen over a wide range of densities. However, the ideal classical model appears not to be applicable. As discussed in Sec. III A 3 and in *Note added in proof*, it is now understood that quantum-mechanical virial corrections are quite important in the so-called "classical-gas" regime of Fig. 5. Therefore, although we consider that it is still useful to continue to label the films as "classical" wherever the heat capacities are Boltzmann-like, it is more correct to add "pseudo" to their name.

Except for very low and high coverages, all films displayed 2D gas signatures for some portion of the experimental temperature range.

The 2D classical-gas phase has not been observed in previous heat-capacity studies on any combinations of adsorbates and adsorbents. Its absence can be ascribed to effects of strong heterogeneity. The appearance of the gas phase in the current studies is one of the strong pieces of

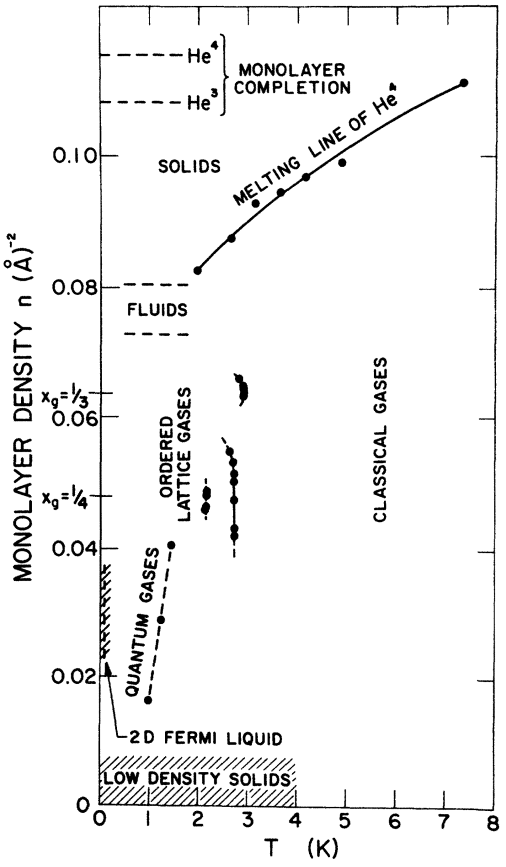

FIG. 5. Phase diagram of helium monolayers on graphite. Identification of several regimes is tentative and subject to revision (see text and *Notes added in proof*).

evidence for uniformity of the Grafoil substrate.

Further implications and quantitative details are described in Secs. III A 2 and III A 3.

2. *Band Structure*

Hagen, Novaco, and Milford[49] have calculated the single-particle band structures and heat capacities of He^3 and He^4 adsorbed on basal-plane oriented graphite at low temperatures. Their results predict that the surface mobility due to tunneling between the substrate sites is extremely rapid, so rapid that there should be little difference between the heat capacities of noninteracting helium on graphite and on a smooth surface. Thus, their calculations and our data agree over wide portions of the phase diagram. It should be noted, however, that the agreement is in a sense one sided: If the calculated bandwidths were greater there would still be agreement, but appreciably narrower bandwidths would not fit the data. Narrower widths would produce modulated band-type heat capacities[49–51] with low-temperature tunneling band peaks. Since such modulation is not seen, the experimental band structure must have a tunneling bandwidth comparable to or larger than the energy gap to the first excited band.

A general criterion for the existence of 2D gas heat capacities in a noninteracting monolayer at low T requires that the site dwell time τ of an adatom satisfies the condition $\tau \gtrsim h/kT$.[50] Therefore, the observation of a 2D gas regime indicates that $\tau \gtrsim 10^{-11}$ s at 4°K. As discussed below, there appear to be appreciable effects due to interactions, but we believe that they are not so large as to invalidate the mobility criterion, at least at relatively low coverages and temperatures near 4°K. However, as we point out in Sec. III C 3, a description of mobility based on a noninteracting model cannot be correct at moderate and high densities, for there the mobility involves collective motion and an interplay between adatom-substrate and adatom-adatom effects. Indeed, it appears that the measurements have not detected any regime in the first monolayer range that strictly corresponds to a noninteracting 2D gas, even at the lowest densities investigated.

3. *Adatom-Adatom Interactions*

If we consider the films by analogy with ordinary three-dimen[illegible]nal (3D) gases then we should expect to obse[illegible] effects of adatom-adatom interactions down to quite low coverages. Actually, even at the lowest experimental coverages the films correspond to quite high equivalent 3D gas densities; e.g., at $x = 0.1$ the mean interatomic spacing is that of a gas at $T = 4$°K and $P = 0.67$ atm. Consequently, the deviations from ideality ought to be appreciable, and it might not be unreasonable to expect significant corrections in heat capacity.

Usually when one considers the effects of interactions the focus is on the equation of state rather than on thermal properties. This is partly because the specific heat is less sensitive; in fact in the very-low-density classical regime the specific heat is not affected by interactions, but remains equal to the ideal gas value.[52] The same result is obtained for 2D gases in the low-density high-temperature limit, where the equation of state can be approximated by a 2D van der Waals equation analogous to the familiar imperfect gas law.[53–55] At appreciable densities, however, the interactions will affect thermal properties as well. If the density is not too great the corrections to the entropy and heat capacity involve only the second virial co-

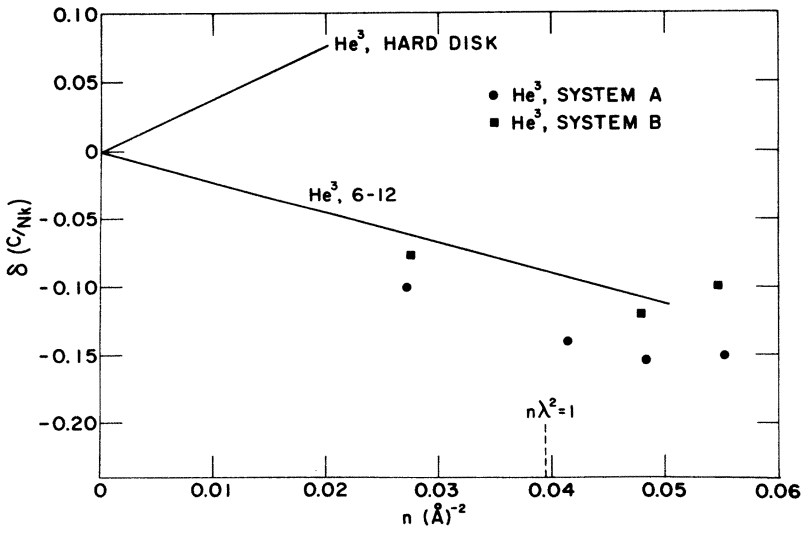

FIG. 6. Deviations $\delta(C/Nk)$ of He^3 specific heats from ideality compared with 2D imperfect gases (Refs. 56 and 57) at $T \simeq 4$°K.

efficient $B(T)$ and higher-order terms can be neglected. The corrections, for both classical and quantum 2D gases, are of the form

$$\delta\frac{S}{Nk} = \frac{S}{Nk} - 2 + \ln(n\lambda^2) = n\beta^2\frac{d}{d\beta}\left(\frac{B}{\beta}\right), \quad (1)$$

$$\delta\frac{C}{Nk} = \frac{C}{Nk} - 1 = -n\beta^2\frac{d^2B}{d\beta^2}, \quad (2)$$

where $\beta = (kT)^{-1}$ and $\lambda = h(2\pi mkT)^{-1/2}$ is the thermal de Broglie wavelength.

Virial coefficients appropriate to helium monolayers at the densities and temperatures of our studies were not available until quite recently. Tabulations of $B(T)$ for classical 2D gases have been published,[54,55] but it has been noted[54] that the classical approximation for 2D He is not appropriate below $T = 100°K$. Very recently, Siddon and Schick[56,57] made fully quantum-mechanical calculations of $B(T)$ for 2D He^3 and He^4. Their extensive study was stimulated by certain questions raised by these experiments, and as will be discussed below, their theoretical results are, at several points, in striking quantitative agreement with the data.

The deviations of the specific heat from the ideal-gas value should be linear in coverage according to Eq. (2), provided that the temperature is high enough to avoid major effects due to quantum degeneracy. The strong condition $n\lambda^2 \ll 1$ could not be met by the experimental densities and temperatures: At 4°K this would require coverages ~1% or less. However, the onset of large changes in the heat capacity of ideal 2D gases begins only at much larger values, $n\lambda^2 \sim 1$. It therefore seems that the experimental coverages were sufficiently low to provide a semiquantitative test of the theory. In Fig. 6 we plot the deviations of the He^3 specific heat from the ideal-gas value versus density; also shown are Siddon and Schick's[57] corrections for the 6-12 potential with He^3 gas parameters. Although there is appreciable scatter and some systematic differences between system-A and system-B data, the measurements seem consistent with a virial correction over the range $n\lambda^2 \lesssim 1$ in moderate agreement with the 6-12 potential. In contrast, the quantum coefficient for hard disk potentials disagrees qualitatively; it leads to positive corrections in the specific heat. At lower densities than $n \simeq 0.025$ the experimental heat capacities deviate markedly from 2D gas behavior; the very-low-density regime is separately discussed in Sec. III E.

Absolute entropies provide an additional basis for comparison, since the entropy correction in Eq. (1) depends on both the magnitude of B and its first temperature derivative, whereas δC measures $d^2B/d\beta^2$. The experimental entropies were obtained by integrating smooth curves drawn through the heat-capacity data, with smooth monotonic extrapolations to the origin below the experimental limit near 40 m°K. Since the experimental values near 40 m°K are quite low and are approximately linear in T, the uncertainty in the extrapolation is not likely to cause a large error in S at 4°K. In Fig. 7 we present the entropy deviations $\delta(S/Nk)$ from ideality for He^3 and He^4 at 4°K. For He^3 we also included in the ideal-gas entropy the nuclear spin term $S_{spin} = Nk\ln 2$; this presumes that the spin entropy is essentially removed at the lowest experimental temperatures (or is accounted for by the extrapolation to $T = 0$) and that the spins are fully disordered at 4°K. Supportive evidence for these assumptions is postponed to later sections.

The data in Fig. 7 exhibit less scatter and better linearity over a wider density range than Fig. 6, a distinction that is probably due to the smoothing effect of integration and the lower sensitivity of the entropy to the temperature dependence of B. We point out that although He^4 entropies follow the density dependence of this virial correction, the He^4 heat capacities do not: This distinction may be due to the particularly high sensitivity of δC to the temperature dependence of B and some residual influence of the low-temperature He^4

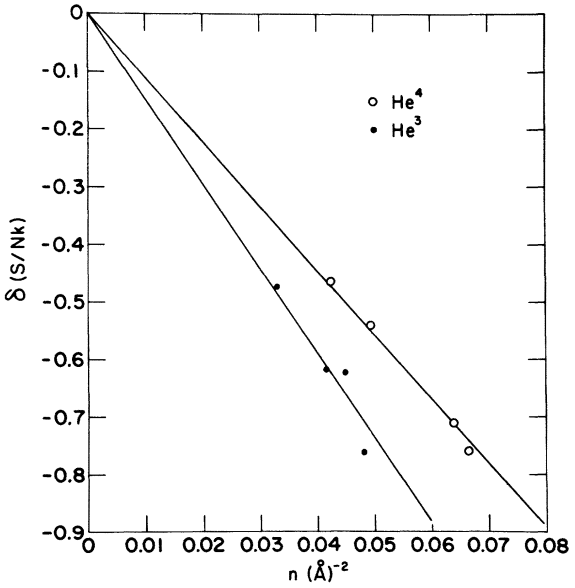

FIG. 7. Deviations $\delta(S/Nk)$ of He^3 and He^4 entropies from ideality at low densities and $T \simeq 4$ °K. The lines are drawn merely to indicate linearity of the deviations. Comparisons of the empirical and theoretical slopes are given in Table III.

anomalies (see Sec. III B 2) extending to 4°K.

Comparisons between the experimental slopes $\delta(S/Nk)$ and $\delta(C/Nk)$ and the theoretical values for hard-disk and 6-12 potentials are given in Table III. We see that the theoretical 6-12 corrections are in moderately good agreement with the measured heat-capacity deviations, whereas the hard-disk model is in qualitative disagreement. The entropy deviations also favor the 6-12 interaction, although the agreement is not good for He^3. In this sensitive comparison it is possible that an appreciable part of the deviation is caused by the manner in which the entropy is extrapolated below $T = 40$ m°K, but at least part of the deviation may be due to real changes in the interatomic potential arising from interactions with the substrate. Presumably, an empirical potential might be constructed which would be consistent with both sets of data, but this has not been done. For more recent developments, see *Note added in proof.*

B. 2*D* Gases: Low-Temperature Regime

1. He^3

Both isotopes at low coverages have specific heats near k/atom in the range $2°K \lesssim T \lesssim 4.2°K$, but stronger departures appear at lower temperature, near the regions where the degeneracy parameter $n\lambda^2 = 1$. Therefore it might be expected that the specific heats could be approximated by theoretical curves for 2D quantum gases.[58] The heat capacity of an ideal 2D Fermi gas has a temperature dependence qualitatively similar to the 3D gas; as T decreases the heat capacity drops monotonically below the classical value, becoming linear in T when $n\lambda^2 \gg 1$. The He^3 films at moderately low coverage and temperatures above 1°K are quite similar to 2D Fermi gases; examples of three such films are shown in Fig. 8. In an early interpretation[1] we fitted ideal 2D Fermi gas curves to each sample, treating the areal density n and the Fermi temperature $T_F(0)$ as fitting parameters,

TABLE III. Virial corrections at 4 °K.

		$n^{-1}\delta(S/Nk)$[a]	$n^{-1}\delta(C/Nk)$
He^3	Experimental	−14.7	−3.0
	Calc., hard disk[b]	−17.53	+3.67
	Calc., 6-12[c]	−7.36	−2.25
He^4	Experimental	−10.4	
	Calc., hard disk[b]	−16.56	
	Calc., 6-12[c]	− 8.12	

[a] Measurements obtained with system B only.

[b] Quantum virial coefficients (Ref. 57) for hard disks of diameter $\sigma = 2.56$ Å.

[c] Quantum virial coefficients (Ref. 57) for 6-12 potential with parameters $\epsilon/k = 10.22$ °K, $\sigma = 2.56$ Å.

where

$$T_F(0) = \pi\hbar^2 n/mk. \tag{3}$$

The fitted ideal gas curves are also shown in Fig. 8. In spite of the close correspondence, the fitting parameters are appreciably different from those calculated from the measured N and the appropriate $T_F(0)$ from Eq. (3). We now believe that the proper explanation is in terms of interactions, as indicated by the very close fit obtained by Siddon and Schick[56] to the data above $T = 1°K$. Nevertheless, the 2D ideal Fermi gas model is a convenient framework for description, and therefore we list the empirical fitting parameters in Table IV. At temperatures below about 1°K the 2D Fermi gas model becomes increasingly inadequate to describe the data. At moderately low coverages the measured heat capacity lies above the theoretical curve fitted to the high-temperature region. The data points form a pronounced "shoulder" in the region $0.1°K \lesssim T \lesssim 0.3°K$ and then tend toward a linear dependence on T at the lowest temperatures. At somewhat higher coverages the shoulder develops into a broad but definite maximum located below 0.1°K. The maximum is most pronounced for density $n \simeq 0.045$ Å^{-2}; at higher densities the heat capacity becomes depressed toward very small values. These features are shown in Fig. 9, which displays only the low-temperature region below $T = 0.5°K$.

The similarity of the low-temperature behavior of the specific heat of the adsorbed film with that of bulk He^3 is remarkable, as can be seen in Fig. 10, which shows that the specific heat of liquid He^3 goes through a broad shoulder before entering the Fermi liquid regime.[59] The specific heat of the solid does not show this shoulder or any anomaly to as low a temperature as has been measured,[60] although it will presumably have some

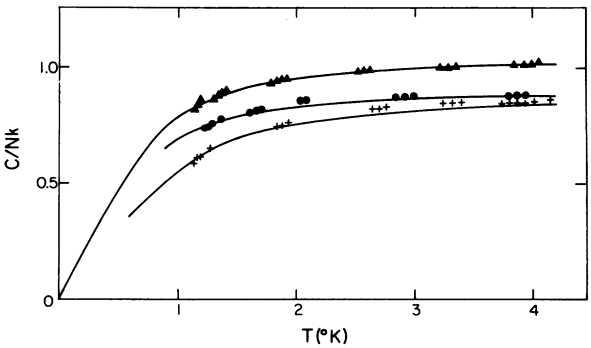

FIG. 8. Specific heats of low-density He^3 films with fitted theoretical curves of ideal two-dimensional Fermi gases. The parameters of the fitted curves are listed in Table IV.

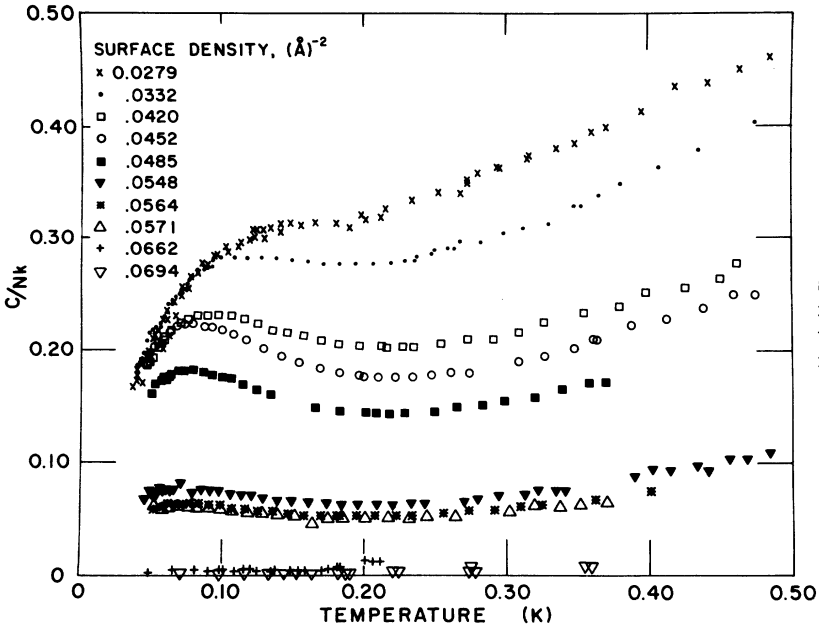

FIG. 9. Low-temperature, low-density specific heats of ten He^3 films showing the anomalies near $T = 100$ m °K and the beginning of the 2D Fermi liquid regime.

kind of anomaly when spin ordering occurs at a few millidegrees.[61,62]

Using the analogy with bulk properties to define film regimes, we call the region of very-low-temperature (almost) linear specific heat a 2D Fermi liquid. The 3D Fermi liquid regime is characterized by an effective mass $m_3^* \simeq 3m_3$; it is obtained by comparing the (almost) linear specific heat with that of an ideal 3D Fermi gas, using the mass as an adjustable parameter. If we treat our data in equivalent fashion and compute an effective mass from the asymptotic linear dependence of the $n = 0.028$ Å^{-2} density film, comparing to the 2D ideal gas specific heat we obtain $m_3^* \simeq (1.7 \pm 0.2)m_3$. Our results in this region are comparable to those obtained by Guo, Edwards, Sarwinski, and Tough[63] in their study of the surface tension of dilute solutions of He^3 in He^4. In their study it was deduced that at low temperatures the liquid surface was covered by monolayer films of He^3. The entropy of the He^3 layers could be deduced from the measured surface tension, using Andreev's theory.[64] The two sets of entropy values agree at the lowest equivalent densities, but diverge at higher density. Perhaps the divergence is due to the difference in substrates; indeed, in view of the differences in substrates and techniques it seems remarkable that the results do agree at any densities and temperatures. Since liquid He^4 presents a disordered but very uniform substrate, the agreement adds to the evidence that graphite is a very uniform substrate and that at low enough coverages the effect of substrate structure in the 2D properties is very small.

The nature of the low-temperature anomaly of bulk liquid He^3 shown in Fig. 10 is unknown. No microscopic theory exists for bulk He^3 in the corresponding region. Several years ago Goldstein[65] correlated specific heat and susceptibility measurements, and concluded that the specific-heat shoulder is due to nuclear-spin ordering in the liquid.[66] Although no susceptibility measurements are yet available for our films, entropy comparisons between He^3 and He^4 seem to indicate that some degree of spin ordering occurs in the experimental range. The assumption that the He^3 spins are ordered at the lowest temperatures was already made in Sec. III A 3, in the evaluation of the entropy correction due to nonideality. It is natural to suspect that the ordering takes place

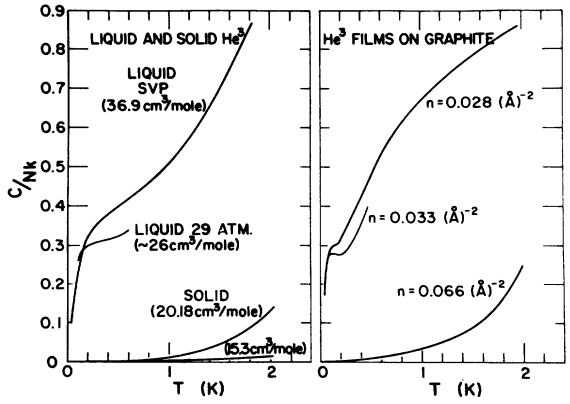

FIG. 10. Specific heats of monolayer and bulk liquid He^3.

in the neighborhood of the low-temperature anomalies, since He^4 does not show this behavior. If this is the case, then the entropy difference $S_3 - S_4$ should show the evolution of the ln2 spin term in the neighborhood of the anomalies (see Fig. 11). The development of a ln2 entropy difference near $T = 0.1°K$ would seem to confirm the conjecture, but it cannot be taken as proof. An alternative interpretation is that the low-temperature anomalies are due primarily to interactions and that the entropy difference is only accidentally equal to ln2. The calculated virial coefficients incline one to this view. (See *Note added in proof.*)

The absolute entropy values are predicated on the assumption that no major specific-heat anomalies occur below the experimental region, for these would be omitted by the extrapolation procedure. Such an omission appears to occur for higher-density films, near the densities of the lattice-gas ordering regime. For further discussion of this regime, see Sec. III C.

2. He^4

As x increases and/or T decreases the He^3 films begin to show appreciable departures from classical gas behavior, but in contrast the He^4 specific heats begin to deviate by increasing above k, rising to form rounded peaks near $T = 1°K$ with varying heights up to nearly twice the classical ideal value. At lower temperatures the specific heats decrease approximately linearly with T, and at the lowest temperatures change to a higher power, approximately quadratic. These features are illustrated in Fig. 12. Results obtained with the two experimental systems are not identical in this portion of the phase diagram. Systems A and B both showed He^4 peaks in this region, but the peak heights of the early B data[4] are appreciably lower than later B runs and all of the A runs. The discrepancies are particularly significant in view of the very close quantitative agreement between all A and B data at other coverages, particularly in the region of the 3°K ordering transition (see Sec. III). It is likely that the disagreement is due to incomplete equilibrium, for we found that the originally weak He^4 anomalies in system B were made stronger by prolonged annealing at relatively high temperatures.

The He^4 results do not resemble the 2D Bose gas, which, except for mass- and nuclear-spin factors, has the same temperature dependence as the 2D Fermi gas.[58] Yet the fact that the He^4 signals rise at just about the same density and temperature at which the He^3 results fall below is a compelling indication that in *both* isotopes the departures must involve statistical effects. The qualitative differences between He^4 films and the ideal 2D Bose gas are therefore probably due to the unrealistic simplifications of the noninteracting model. In the following paragraphs we compare the He^4 results with predictions of several theoretical models of Bose films.

It is well known that although there is no long-range momentum order in 2D Bose fluids above $T = 0$,[67] the restriction to finite geometry allows ordering to occur at some finite temperature T_0.[68–75] It seems unlikely that the experimental anomalies can be caused by size effects, i.e., if the film is composed of noninteracting domains which are so small as to cause the peaks near 1°K. The existence of a finite ground-state occupation at a finite accumulation temperature T_0 does not imply that the ordering will be accom-

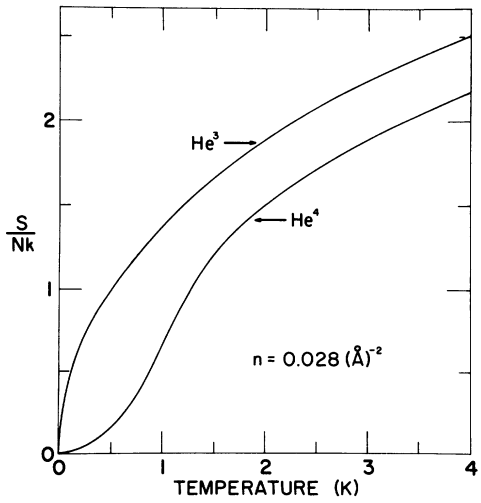

FIG. 11. Calculated entropies for equal density ($n = 0.028$ Å^{-2}) He^3 and He^4 films. The entropy difference between the two isotopes develops to approximately ln2 after the He^3 low-temperature specific-heat anomaly.

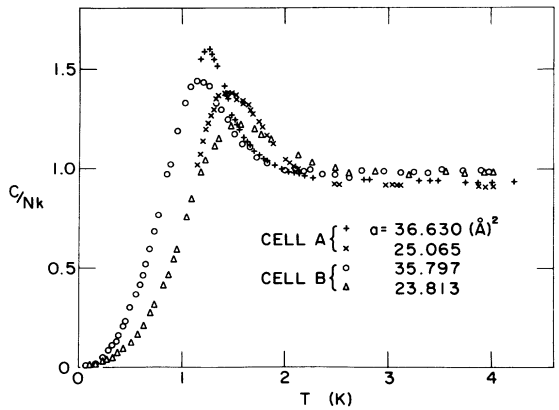

FIG. 12. Specific heat vs temperature for He^4 samples in the 2D gas regime.

panied by any marked changes in the heat capacity. Indeed, the specific heat of an ideal 2D Bose gas remains relatively unaffected by size restriction down to quite small dimensions. Calculations for mass-4 bosons at liquid-He^4 density on a 270-Å square plane show that $C(T)$ is similar to the infinite 2D gas.[71] An anomaly due to size restriction probably does not appear until dimensions are a few Å, when the single-particle energy-level spacing becomes comparable to kT.[70] The effective dimensions of the domains in our films appear to be at least several hundred Å (see Sec. III C).

In slab geometries of finite thickness the ideal Bose gas exhibits a heat-capacity anomaly.[71,72,75] The anomalies are pronounced and occur at temperatures above that of the corresponding 3D transition. These results do not seem applicable to monolayers. In addition to the extreme simplicity of the model, the theory requires that the thickness be a few Å or more for T_0 to be as high as 1°K, whereas in the He-graphite system the higher surface-normal excitations are virtually unoccupied at liquid-helium temperatures,[49] and thus the effective thickness of the films is virtually zero.

Several possible explanations of the He^4 specific-heat anomalies have appeared since our experimental results were first reported. Campbell, Dash, and Schick[76] suggested that they are associated with film-density changes in weak lateral fields due to long-range gradients in the substrate binding energy. They showed that the ideal Bose gas develops pronounced heat-capacity peaks in quite small fields and they obtained a reasonable fit to the data by assuming a variation of about 0.6% in the substrate binding energy.

Widom and Sokoloff[77] reinterpreted the lateral-field model as indicating remnant Bose condensation and pointed out some implications for the spreading-pressure and vapor-pressure isotherms. Their predictions were tested by Elgin and Goodstein[47] through measurements of vapor pressure and heat capacity of He^4 on Grafoil. The results were found to be at variance with the predictions of the model.

Novaco[78] proposed that the He^4 peaks could be evidence for lateral evaporation of a two-dimensional liquid ground state, together with a smearing effect due to weak substrate inhomogeneities. Model calculations resulted in strong anomalies located near $T=1$°K. The absence of peaks in He^3 films was attributed to a much weaker or nonexistent binding of the lighter isotope.

Siddon and Schick[56,57] find that the second virial coefficients $B(T)$ of 2D He^4 with 6-12 interactions lead to pronounced increases in the heat capacity as the temperature is reduced toward $T=1$°K. Their theoretical results are in close quantitative agreement with the measurements over the entire temperature range above the peaks. Their theoretical curves continue to rise at lower temperatures, however. This region of disagreement with the experiments is ascribed to the importance of higher-order terms in the virial expansion. A strong argument for the applicability of the Siddon-Schick calculation is the comparable success of their results in fitting the He^3 data with virial coefficients appropriate to that isotope. It therefore appears that the low-coverage regime can be understood in terms of uniform 2D systems, with no necessity for invoking substrate heterogeneity. However, before one can accept the virial correction as a complete explanation, additional experimental facts need to be mentioned. (Also see *Note added in proof.*)

A small disagreement remains between A and B data, even after careful annealing and remeasurement. The disagreement appears to be significant in view of the generally better correspondence between systems A and B, especially in the region of the ordering peak at $x_g=\frac{1}{3}$ (see Sec. III C).

An additional qualification emerges from our failure to observe He^4 anomalies at coverages slightly greater than one completed layer, where the second-layer densities are comparable to the partial first-layer films. (However, see *Note added in proof.*) A strict interpretation of the He^4 peaks as due to ordinary pair potentials between adatoms on an inert smooth substrate would suggest that the second layer should behave similarly, since the underlying first layer preserves its 2D solid character (see Sec. III D). Thus, it seems possible that there is some substrate contribution to the physics of the film; this may be of the lateral-field type, or perhaps via mediation of the adatom-adatom interactions.[15,79]

C. Lattice Gases

1. *Observations*

In the density range $0.05\ \text{Å}^{-2} \lesssim n \lesssim 0.07\ \text{Å}^{-2}$ the films undergo second-order phase transitions to

TABLE IV. He^3 films compared with ideal 2D Fermi gases.

Sample density n Å^{-2}	$T_F(0)_{\text{calc}}$ [a] °K	$T_F(0)_{\text{fitted}}$ °K
0.0154	0.783	3.6
0.0273	1.39	3.4
0.0415	2.11	4.8

[a] Computed from Eq. (3) with atomic mass m_3 and measured density.

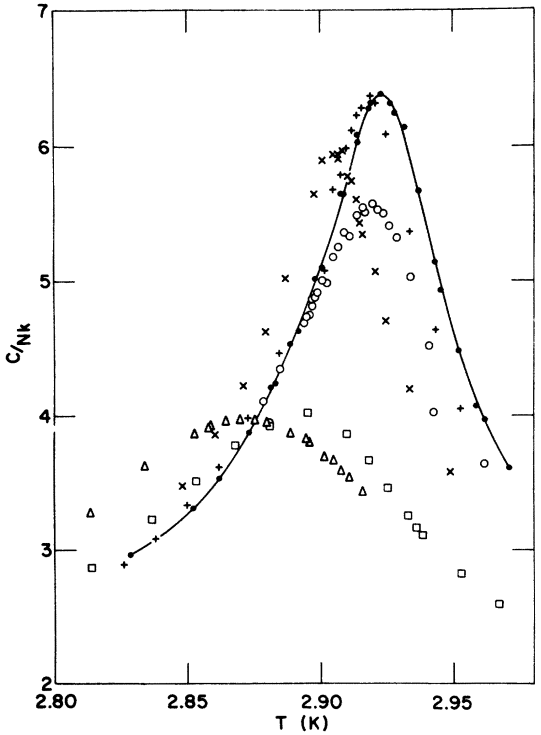

FIG. 13. Critical regions of lattice-gas ordering transitions of several samples of He^4. Densities n $Å^{-2}$ are △, 0.0607; ○, 0.0631; ●, 0.06366 ≡ n_c; +, 0.0641; ×, 0.0647; □, 0.0656.

ordered lattice-gas arrays. Our identifications of these regimes are based upon certain correspondences between the experimental heat capacities and theoretical models. We also note observations of ordering in other adsorption systems, and we cite very recent results from a study of nuclear-magnetic resonance of He^3 films which supports our identification. In this section we first present the experimental evidence, then

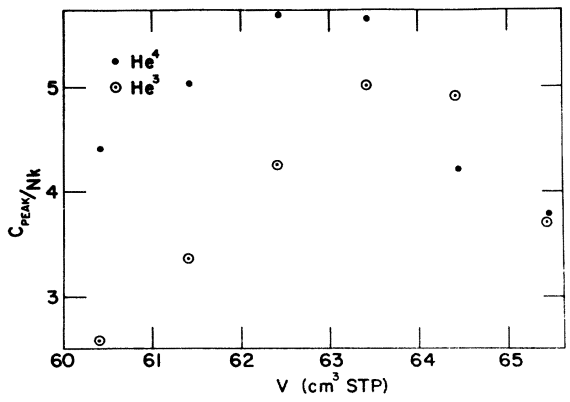

FIG. 14. Peak height vs gas quantity near critical ordering density, for cell B.

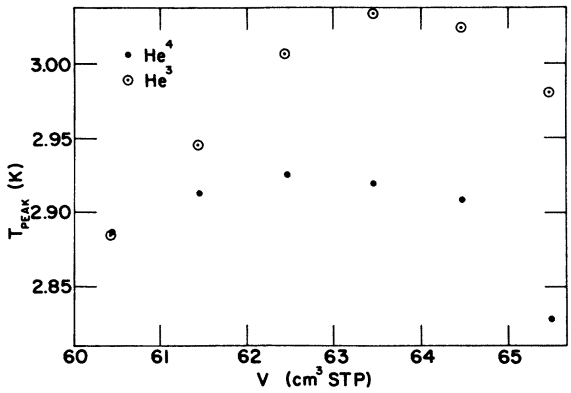

FIG. 15. Peak temperature vs gas quantity near critical ordering density, for cell B.

the measurements are compared with existing theory, and we discuss new questions raised by the experiments.

The gross features of the ordering regimes involve the emergence of strong and sharp heat-capacity peaks in both isotopes within relatively narrow ranges of temperature and coverage. Peak heights are extremely sensitive to coverage; peak temperature somewhat less so. In Fig. 13 we show the peak regions of He^4 films at coverages near $n = 0.07$ $Å^{-2}$. We find very similar behavior in He^3. The variations of peak height and tem-

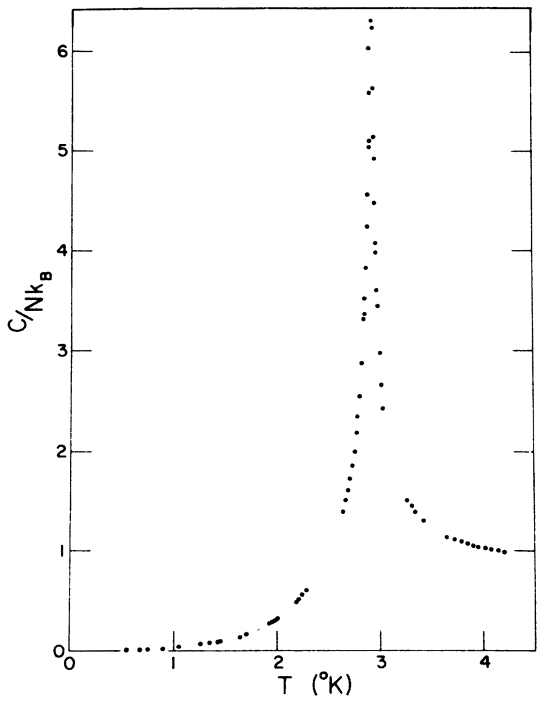

FIG. 16. Specific heat of He^4 at critical density n_c. Data obtained with system A.

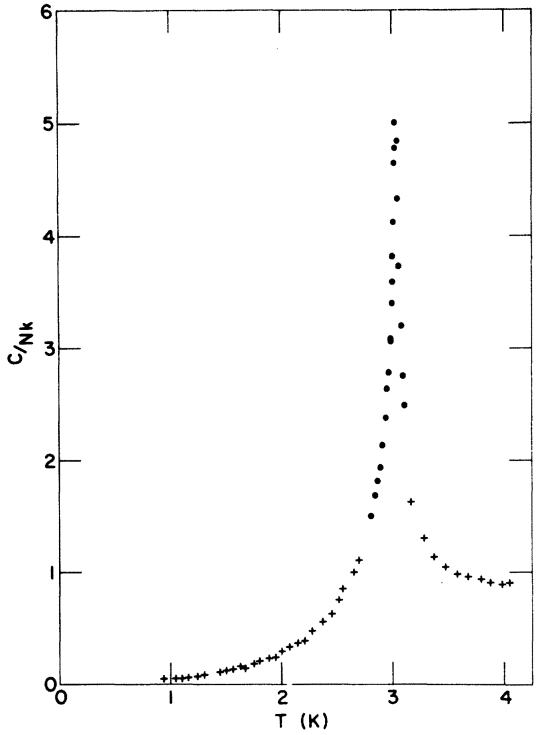

FIG. 17. Specific heat of He^3 at critical coverage. Data obtained with system B. Densities n Å^{-2} scaled from n_c (He^4) are ●, 0.0643; +, 0.633. Since the 0.0643-Å^{-2} sample was only measured near T_c, we show a composite with a nearly critical density sample at higher and lower temperatures.

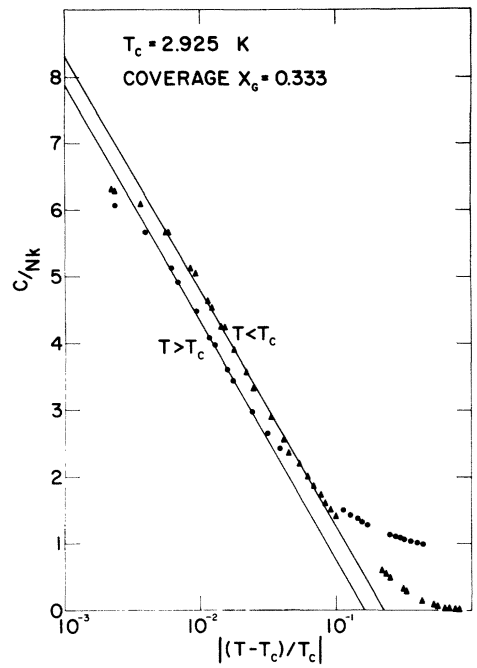

FIG. 18. Logarithmic dependence of the specific heat of He^4 at $x_g = 1/3$ in the critical region.

perature with coverage are illustrated in Figs. 14 and 15.

The full curves for He^3 and He^4 at critical density n_c are shown in Figs. 16 and 17. The sharpness of the peaks provided extremely sensitive gauges of reproducibility, yet we were able to repeat these results in different runs in the same or different calorimeters. Furthermore, similar peaks were obtained for He^4 in a third Grafoil cell in a completely independent calorimeter.[80]

The peak regions of the critical coverage samples can be described by power-law temperature dependences of the form

$$C \propto |t|^{-\alpha}, \quad t \equiv (T - T_c)/T_c, \tag{4}$$

with empirical exponents $0 < \alpha < 0.3$ depending on the extent of the critical region over which the data were fitted. For $\alpha = 0$ the power law reduces to logarithmic form

$$C/Nk_B = -A \ln|t| + B, \tag{5}$$

and in Fig. 18 we show the data for a critical-coverage He^4 film on a logarithmic scale. Equation (5) is obeyed over slightly more than one decade in t on both sides of T_c, extending out to $|t| \simeq 0.1$. We evaluated the empirical coefficients for high- and low-temperature branches separately for both isotopes, and the results are listed in Table V.

It is noteworthy that the critical quantities n_c,

TABLE V. Critical parameters of lattice-gas ordering transitions of He monolayers on graphite and of exact theoretical models. [Quantities A and B refer to Eq. (5) in text.]

System	x_c	$A(T>T_c)$	$A(T<T_c)$	$B(T>T_c)$	$B(T<T_c)$
He^4	$\frac{1}{3}$	0.527 ± 0.001	0.521 ± 0.004	−0.982	−0.801
He^3	$\frac{1}{3}$	0.431 ± 0.002	0.427 ± 0.004	−0.785	−0.637
Quadratic [a]	$\frac{1}{2}$	0.4945	0.4945		
Triangular [b]	$\frac{1}{2}$	0.4991	0.4991		
Honeycomb [a]	$\frac{1}{2}$	0.4781	0.4781		

[a] Attractive and repulsive nearest-neighbor interactions.
[b] Attractive interactions only; no transition for repulsive interactions.

T_c for the two isotopes are approximately, but not precisely, the same. We were particularly troubled by the implications of an isotopic difference in n_c, and we carried out a special series of experiments on both He^3 and He^4 in system B in order to eliminate systematic errors. As a result of this series the difference, amounting to an excess of about 1.5% for He^3, is very well documented. In this series we also compared critical temperatures for both He^3 and He^4: Here, too, a slight isotopic effect was confirmed. The significance of these isotopic differences is discussed in Sec. III C 2.

Outside of the critical region the two branches become quite distinctive. On the high-temperature side the specific heat of both isotopes approaches k near $T=4°K$. At low temperatures the signals decrease rapidly; they can be described approximately by an exponential dependence of the activation type, with an activation energy $\simeq 2°K$ (see Sec. III C 3). It can also be described by an empirical law of the form $C \propto e^{aT}$ over a rather wide range, $0.5°K \lesssim T \lesssim 2.5°K$. This relation is curious, and we do not know its significance.

At densities above and below n_c the peaks diminish in height and shift to lower temperature. The behavior at $n > n_c$ is quite different than $n < n_c$. Above critical density (only He^4 has been examined at coverages much above n_c) the peaks become steadily smaller and broader, disappearing entirely by $n \simeq 1.17 n_c$. Below critical coverage we find peaks of some sort persisting down to $n \simeq 0.7 n_c$. In addition we found two distinct classes of peaks near $n = \frac{3}{4} n_c$. These peaks appeared on different runs, the higher-temperature peaks occurring on earlier runs of both cells, whereas there had been no evident differences in the manner of preparation for the runs or in taking of data. The two classes differ in peak shape. Examples of both classes are shown in Fig. 19. It must be emphasized that because of these differences we studied this region of coverages particularly carefully in both systems. The phase diagram in Fig. 5 shows both lines of peaks, although the existence of these phases is not well established and further experimentation is necessary to elucidate whether the different peaks are due to cell changes occurring within a year's period or to the two configurations discussed in Sec. III C 2.

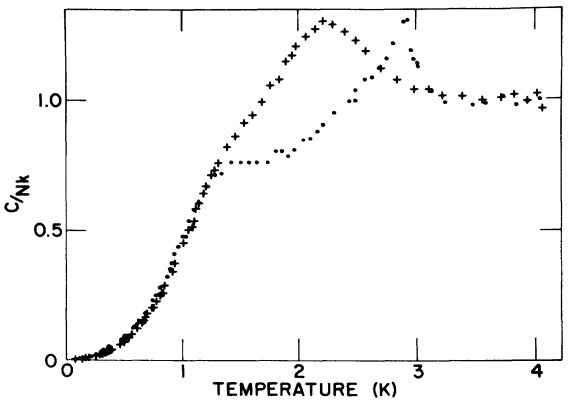

FIG. 19. Examples of the two types of anomalies seen in He^4 films at $x_g \simeq \frac{1}{4}$.

2. *Interpretations*

As mentioned earlier, we believe that the sharp 3°K peaks are due to second-order phase transitions to ordered monolayer structures in registry with the substrate. First we discuss the direct evidence for registered monolayers obtained by low-energy-electron diffraction (LEED). Several such phases have been identified in LEED studies of physisorption. Of particular relevance to our present study is the investigation by Lander and Morrison[81] of structures of films adsorbed on basal planes of graphite. Among those structures are two that we believe are particularly relevant to films of He on graphite. In Fig. 20 are illustrated a triangular array with atomic spacing twice that of the graphite hexagons, observed in Cs monolayers, and a triangular $\sqrt{3}\,R\ 30°$ array seen in Xe films. We also show a rectangular $\sqrt{3} \times 2$ arrangement. Although Lander and Morrison did not report such a structure in their LEED work, we believe that it may occur in He films at appropriate coverages. The LEED results for Xe are particularly interesting. The ordered $\sqrt{3}\,R$ 30° state was seen at nearly completed monolayer densities and liquid-nitrogen temperatures; as T increased, the diffraction pattern became fainter and finally disappeared above about 90°K. Above this temperature the diffraction corresponded to an amorphous "liquid." Lander and Morrison suggested that the change from the ordered to the disordered state is a second-order phase transition.

We believe that the sharp peaks in He monolayers at $n \simeq 0.06$ Å^{-2} do indicate second-order phase transitions to ordered arrays having the same structure as the $\sqrt{3}\,R$ 30° phase seen in the LEED study of Xe films. The He-film densities agree with the density of the $\sqrt{3}\,R$ 30° arrangement to within the uncertainty of our measurements of adsorbent areas. The relative densities can be expressed in terms of the fraction x_g, defined by

$$x_g \equiv N(\text{adatoms})/N_s(\text{sites}),$$

where N_s(sites) refers to the number of hexagonal adsorption sites on the graphite substrate. The triangular $\sqrt{3}\,R$ 30° arrangement corresponds to

$x_g = \frac{1}{3}$. Now we compare the x_g values for He^3 and He^4 at critical coverage x_c, calculated according to the crystallographic parameters of graphite[82] and the substrate areas determined by argon adsorption isotherms (see Sec. II): these values are

system A: $x_g(He^4) = 0.35$,

system B: $x_g(He^4) = 0.310$, $x_g(He^3) = 0.315$.

The relative values are uncertain to about 10% due largely to the estimated uncertainty in the effective molecular area of argon, which is derived from the density of solid argon.[21] In addition, the measurement of adsorption area of System A was less carefully made: The difference in techniques can account for much of the variation. We therefore find that the densities of the films possessing the logarithmic heat-capacity peaks are consistent with $x_g = \frac{1}{3}$. With this identification and the area 5.2361 Å^2 of a primitive hexagon on the basal plane of graphite,[82] the critical density n_c is calculated to be 0.06366 Å^{-2}. All other sample densities are computed by scaling the volumetric quantities relative to the critical quantities for He^4 in each cell.

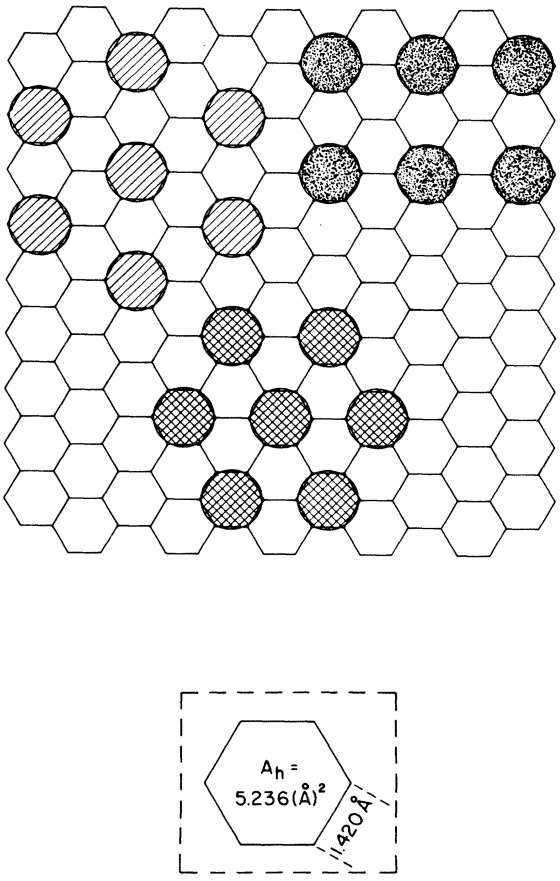

FIG. 20. Three possible ordered epitaxial structures of monolayers adsorbed on basal-plane graphite. The two structures on top have relative density $x_g = \frac{1}{4}$; the lower structure has $x_g = \frac{1}{3}$. Atomic sizes correspond to the He diameter $\sigma = 2.56$ Å.

The identification of the logarithmic peaks as due to lattice-gas ordering indicates that the low-temperature phase must be a regular array of atoms localized on substrate sites. In sharp contrast, however, the heat capacity at $T = 4$°K corresponds to a 2D mobile gas. Thus, at this stage one is led to an interpretation of the peaks as due to a transition in both the spatial order and the mobility. These indications are buttressed by entropy comparisons, as follows: If the atoms are completely localized in sites, the He^4 entropy should fall to very small values in the experimental range, whereas the He^3 entropy should retain a spin contribution down to some very low temperature of nuclear-dipole interaction. Thus, since the spin entropy of He^3 is constant over the experimental range, there should be little distinction between the experimental entropy differences of the two isotopes in the ordered phase. This is indeed what is found: In Fig. 21 we see that the values for He^3 and He^4 around $x_g = \frac{1}{3}$ are nearly the same, distinct from the behavior at lower coverages. Figure 21 also includes data of Elgin and Goodstein,[83] who obtained entropy values for He^4 on Grafoil by combined vapor-pressure and heat-capacity measurements. Their 4°K values are in excellent agreement with ours.

Direct evidence of localization has recently been obtained by Rollefson,[84] using NMR techniques. This study was conducted on He^3 films on graphitized carbon black: As noted earlier, this material has purely basal-plane adsorption surfaces and

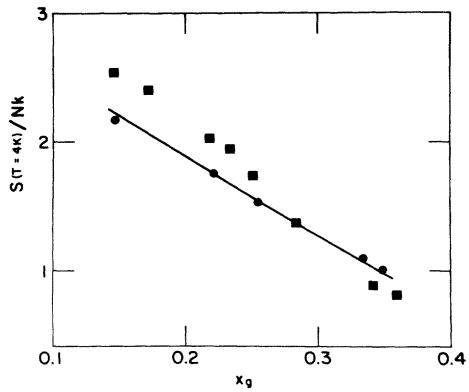

FIG. 21. Calculated entropies at $T = 4$ °K for several coverages, obtained from our smoothed measured specific heats. ■, He^3; ●, He^4. Solid line He^4 from Elgin and Goodstein, Ref. 83 of text.

shows adsorption isotherms similar to exfoliated graphite. Rollefson observed changes in linewidth versus coverage and temperature which correlate closely with the mobility changes deduced from our heat capacities. At a coverage corresponding to the $x_g = \frac{1}{3}$ transition the linewidth between 3 and 4°K was approximately constant, but began to increase at lower T. The width tended toward a constant low-temperature value which is consistent with the dipolar broadening of He^3 fixed at distances corresponding to the $x_g = \frac{1}{3}$ lattice. At slightly higher and lower coverages there was little or no increase in the linewidth at low T. The reductions in linewidth are interpreted as motional narrowing due to atomic mobility; thus the low-temperature state of the critical coverage film is localized, whereas at higher temperatures it is mobile, and for coverages higher and lower than critical the films remain mobile at all temperatures investigated. Additional evidence for localization is discussed in Sec. III C 3.

Now we consider the two classes of heat-capacity peaks that occur at somewhat lower densities than n_c. Using the same calibration of area as before, these densities correspond to an atom-to-site ratio $x_g \simeq \frac{1}{4}$. It is appealing to speculate that the two classes of peaks at $n \simeq \frac{3}{4} n_c$ correspond to the two different structures possible at $x_g = \frac{1}{4}$. They are relatively easily transformed from one into the other (by shifting alternate rows of atoms), which might account for the unpredictable appearance of either class of specific-heat peaks in any particular run. A further point is that the relatively low density of these arrays would permit considerably higher mobility than at $x_g = \frac{1}{3}$. This is consistent with the fact that the heat capacities at $x_g = \frac{1}{4}$ do not fall quickly at $T < T_{\text{peak}}$, but rather retain considerable gaslike character at lower temperatures.

3. *Comparisons with Theory*

There are strong similarities between the transitions in the experimental films and certain theoretical models. Fowler[85] studied a classical monolayer of atoms localized on a regular array of adsorption sites, and showed that in the Bragg-Williams approximation the system can undergo a first-order phase transition to a dense ordered array. Peierls,[86] in an improved (Bethe-Peierls) approximation, obtained a similar result. Several subsequent authors studied the model and pointed out its similarities to a two-dimensional spin-$\frac{1}{2}$ Ising system. Onsager[87] gave the exact and complete solution for rectangular arrays with nearest-neighbor interactions. Exact solutions now exist for triangular, honeycomb, and Kagomé lattices with attractive (ferromagnetic) and repulsive (antiferromagnetic) nearest-neighbor interactions.[88–90] The exact solutions show that the transition is second order. In the critical region the heat capacity has a logarithmic temperature dependence, having the form of Eq. (5). The theoretical coefficients A, which are listed in Table IV, are similar in the different lattices. All of the solutions refer to the case of zero external magnetic field, which corresponds in the lattice-gas model to a relative coverage $N_{\text{atoms}}/N_{\text{sites}} = \frac{1}{2}$.[91] There is no transition for triangular and Kagomé arrays with repulsive interactions: In these cases there is no ordered arrangement at coverage $\frac{1}{2}$. However, an ordered arrangement is possible for a triangular array with repulsive interactions at coverage $\frac{1}{3}$. Campbell and Schick[92] studied the properties of a classical triangular lattice gas having strong nearest-neighbor repulsions and weak second-neighbor attractions, using the Bethe-Peierls approximation. They found ordering in the vicinity of one-third coverage, and no ordered state at one-half. The ordering transitions were found to be first order, which is a typical artifact of the Bethe-Peierls approximation; however, it could also be caused by the assumed attractions (see comments below).

The experimental coefficients A for both isotopes at temperatures above and below T_c are compared with the theoretical values in Table V. It should be noted that the correspondence between the Ising model and the lattice gas involves $N_{\text{spins}} \rightarrow N_{\text{sites}}$[91]; thus the experimental coefficients in Table V correspond to values of A for $N_s = 3N_{\text{He}}$. The quantitative agreement was unexpected: It seems remarkable in view of the differences between the models and the physical systems. The critical coverage in the films is $\frac{1}{3}$. Higher-density ordered phases are apparently ruled out by the large repulsive energy of He atoms on nearest-neighbor sites. The interactions between second-neighbor and more distant *localized* He atoms are attractive, for if the atoms are localized the interaction is due only to the potential energy, and unless the interaction between the atoms on the surface is markedly different from the gas, the long-range potential is attractive. But if the He is not localized the zero-point energy due to He-He collisions must also be taken into account. The zero-point energy in bulk liquid He is so large that it nearly cancels the attractions: The net binding in liquid He is much lower than that due to the potentials alone. It is clear that one cannot treat the He atoms on graphite as localized by the graphite site potential alone. This is obvious from the gaslike character of the heat capacities at lower coverage. Furthermore, the heat capacity of the films at *critical coverage* shows gaslike character

near 4°K: Instead of falling monotonically to zero at temperatures above T_c, the signals tend to the value k/atom. Also, if at critical density $\frac{1}{3}$ the interactions were attractive, as they would be if zero-point energy were unimportant, the array would have a finite binding. This would cause condensation into $x_g = \frac{1}{3}$ clusters at lower densities; whereas we have not observed such a first-order phase transition. Thus, the atoms are not localized as in the usual theoretical model.

Summing up the indications concerning the nature of transition, we conclude that the actual transition involves a fundamental change in the mobility as well as in the spatial distribution. The mobility evident at 4°K in these relatively high-density films has to be understood as a collective property of the interacting film on a structured surface, and not as single-particle mobilities of a conventional band model. The transition in mobility seems analogous to the Mott transition[93] between insulating and conducting states of electrons in metals, but of course the nature of the forces and the physical parameters is entirely different.

The fact that the temperature dependence of C at temperatures well below T_c tends toward an activation-energy form is qualitatively consistent with localized lattice-gas models. The theoretical asymptotic low-T expression[89] is

$$\frac{C}{Nk} \simeq \left(\frac{a_1 T_c}{T}\right)^2 \exp\left(\frac{-a_2 T_c}{T}\right). \tag{6}$$

For quadratic and triangular arrays, $a_1 = a_2 \simeq 3.3$. Fitting Eq. (6) to the He^4 $x_g = \frac{1}{3}$ data in the low-T range we obtain empirical parameters

$$a_1 = 0.138 \pm 0.004, \quad a_2 = 0.763 \pm 0.004$$

for $0.538°K < T < 0.681°K$. There were only six data points in this region: At higher T the heat capacity deviates monotonically above the analytic law, and at lower T the heat capacity is too small for reliable measurements. Thus, the experimental range for Eq. (6) was extremely narrow and the data are scanty. Nevertheless, we feel that the discrepancy between experimental and theoretical parameters in this region is important because it contrasts so sharply with the close agreement near T_c.

The theory of the Ising model contains an interesting prediction as to the heat capacity of finite systems. Onsager[87] showed that in a "one-way infinite" quadratic array of $n \times \infty$ spins, the specific-heat peak is rounded, and that the logarithmic term in Eq. (5) has the limiting value

$$C_{max}/Nk \sim A' \ln(n), \tag{7}$$

where A' has the same value as the coefficient A in Eq. (15). Ferdinand and Fisher[94] studied $n \times m$ arrays: They found that the peak heights tend to the Onsager limit for large n, m and are not strongly dependent on the ratio n/m. These predictions seem relevant to the current experiments in view of the quantitative agreement between the experimental and theoretical coefficients A. Thus, if we assume that A' is as insensitive to lattice structure as is A, then Eq. (7) can provide a gauge of the effective sizes of the experimental films. In the actual films it would be most unlikely for the entire sample to act as one thermodynamic entity. Optical microscopy indicates uniformity over dimensions ~3 μ, but important irregularities invisible to the optical microscope could easily break up the surface into smaller uniform regions: Thus 3 μ is probably an upper limit to the effective size of the film "domains." That seems borne out by the numerical result: according to Eq. (7) with the experimental A' and n corresponding to 3 μ, $C_{max}/Nk \simeq 14$. The experimental maxima are less than half of this value, the highest measurement being 6.4 for He^4 in system A. The discrepancy can be due to the fact that the actual domains are much smaller than the optically uniform regions: They would have to be about 100 times smaller. But it is likely that at least part of the discrepancy is due to slight nonuniformity within each domain; this would also cause rounding of the peaks.[95] The present state of the theory and of our inadequate characterization of the films prevent us from going any further.

Finally, we consider the small isotopic differences of the critical paramters: $T_c(He^3)$ is higher than $T_c(He^4)$ by about 80 m°K, and $N_c(He^3)$ is 1.5% greater than $N_c(He^4)$. The temperature shift has been considered recently by Siddon and Schick.[96] The isotopic dependence cannot be accounted for by differences in the potential energies of the He-He or He-graphite interaction. Therefore, the strictly classical localized theories are inadequate. Using a pseudospin formalism to introduce quantum effects, Schick and Siddon showed that the shift can be accounted for by a slight difference in the net He-He interactions of the two isotopes probably arising from the mass dependence of the probability distributions of the atoms in each site.

The isotopic dependence of N_c, although small, is significant, and cannot be accounted for in simple lattice-gas models. The He^3 excess is far greater than the amount of additional He^3 in the vapor phase, and the difference is opposite to what might be attributed to a small fraction of strong binding sites. We believe that it is due to a finite occupation of the second layer. He^3 has a lower binding energy to the substrate and a lower

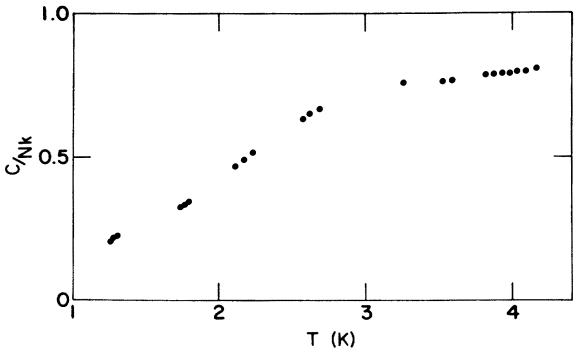

FIG. 22. Specific heat of the 2D liquid at $n = 0.075$ Å^{-2}.

maximum density in the first layer. Therefore, the occupation of the second layer of He^3 at the critical point is greater than of He^4: The higher value of T_c for the He^3 is an additional factor tending to increase its second-layer Boltzmann factor. Also, the localized array at critical coverage provides deeper sites for second-layer adsorption than exist on a completed first layer. These considerations imply that the second-layer occupation of He^4 is probably not negligible, but smaller than that of He^3. Thus the critical coverage of neither isotope can be taken as an exact measure of the adsorption area, but it is probably within 1% for He^4. Therefore, although the critical quantity of He^4 provides a precise area and density calibration, it remains subject to a small uncertainty in absolute value.

D. He^4 at High Densities

1. 2D *Fluid Phase at* $n > n_c$

All evidence of the ordering peak in He^4 disappears when the density is increased above $n \simeq 0.07$ Å^{-2} (a detailed study of high-density He^3 was not made; however, such a study is now in progress[97]). At $n = 0.080$ Å^{-2} the heat capacity is a smooth monotonic function over the explored range 0.73–4.2°K, as shown in Fig. 22. Its temperature dependence at $T > 1$°K can be written as a power series in T, with terms to third order. Near 4°K the specific heat is nearly constant at $C/Nk \simeq 0.8$. We believe that this phase corresponds to a 2D fluid or dense gas. At these densities there can be no simple registry with the graphite lattice, and although the amplitudes of the atomic wave functions must be greater over the centers of the graphite hexagons, the particles cannot be localized on the sites. The misregistry should permit considerable mobility at low tempertures. Owing to the high density this mobility involves the coordinated motions of neighboring molecules, as in ordinary three-dimensional liquids. The interactions between the molecules are also responsible for the fact that the heat capacity does not approach the ideal-gas value at the higher temperatures. The difference between the experimental entropy at 4°K and the ideal-gas value is consistent with the trend of the virial corrections at lower coverages.

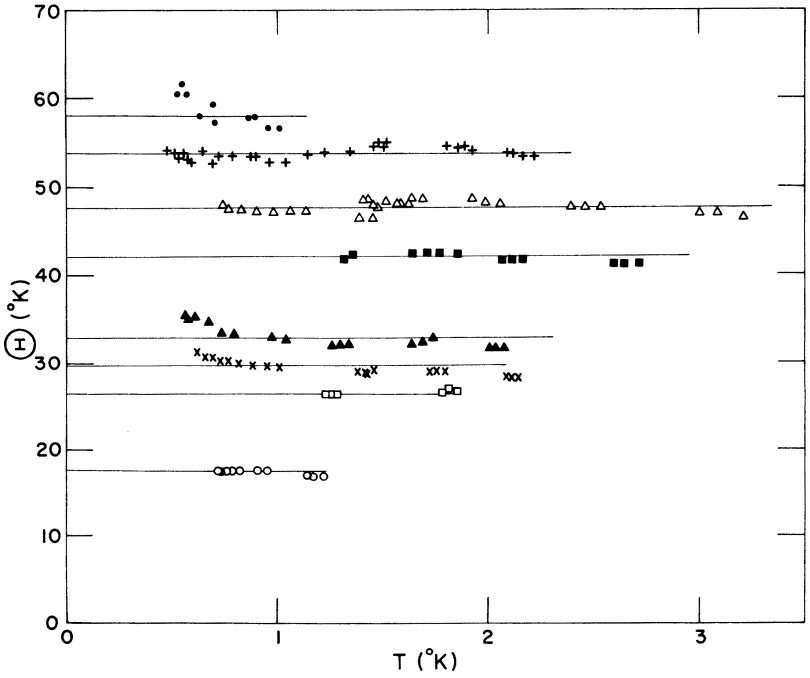

FIG. 23. 2D Debye temperatures for high-density He^4 films. Densities n Å^{-2} are ○, 0.0824; □, 0.0927; ×, 0.0942; ▲, 0.0991; ■, 0.104; △, 0.108; +, 0.113; ○, 0.115.

2. 2D *Solids*

As coverage is increased still further the heat capacities develop quadratic temperature dependences at low T, indicative of 2D solid behavior: even the sample at $n=0.075$ Å^{-2}, which is believed to be fluid at higher temperatures, has an appreciable T^2 region below 1°K.

The low-temperature T^2 regions were analyzed in terms of a 2D Debye model. We assumed harmonic transverse and longitudinal branches with no dispersion and a sharp cutoff of the density of states at a frequency $\omega_{max}=k\Theta/\hbar$ such that the total number of normal modes is equal to $2N$. Empirical values of the characteristic temperatures Θ were obtained by comparisons with numerical calculations of the 2D Debye integral. The empirical Θ's were found to be nearly independent of temperature up to $T/\Theta \simeq 0.07$, consistent with the range of validity of the low-temperature asymptotic formula

$$C/Nk = 28.8(T/\Theta)^2. \tag{8}$$

At higher temperatures deviations from Eq. (8) can be expected due to the different speeds of sound of the two branches even if the simple phase-space density of states remained correct. In Fig. 23 we show the empirical $\Theta(T)$ for each sample. For the two highest densities the range of constant Θ is more restricted. At the highest coverage Θ is not constant over any interval. Its trend is consistent with effects of thermal excitation from the first to the second layer, which will be discussed later.

Table VI lists the experimental values of $\Theta(T=1°\text{K})$ for the several samples. The monotonic trend of Θ with density is similar to the behavior of bulk solid helium. The correspondence is put on a more quantitative basis in Fig. 24, where we show the film values together with Ahlers's[98] measurements of 3D Debye characteristic temperatures of hcp He^4 on a common scale. The equivalent molecular area of the hcp solid is taken as (molecular volume)$^{2/3}$. Although particular models[99,100] of 2D and 3D solid He exhibit similar Θ's this degree of correspondence is unexpected. (See *Note added in proof.*)

TABLE VI. 2D Debye Θ's and "melting" peak temperatures of He^4 monolayers.

Density n, Å^{-2}	Θ at $T=1$°K, in °K.	T_p in °K
0.0823	17.6	1.93
0.0873		2.65
0.0927	26.7	3.12
0.0942	29.8	3.65
0.0967	33.0	4.11
0.0991	37.6	4.7
0.1037	42.2	5.7
0.1079	47.8	6.8
0.1134	53.9	
0.1150	56.1	7.36
0.1327 [a]		7.86

[a] Greater than completed monolayer density, but the peak for the solid-fluid transformation of the first layer is still present. The slight increase in T_p above that for $n=0.1150$ Å^{-2} is attributed to a small density increase due to compression by the second layer.

Since the film and bulk solid Θ's coincide over the common range their Grüneisen parameters are also the same. Defining the 2D parameter γ_{2D} in analogy with γ_{3D} by

$$\gamma_{2D} \equiv -\frac{\partial \ln(\Theta_{2D})}{\partial \ln(a)}, \quad \gamma_{3D} \equiv -\frac{\partial \ln(\Theta_{3D})}{\partial \ln(v)}, \tag{9}$$

one obtains from the equality of Θ's at equivalent densities

$$\gamma_{2D} = \tfrac{3}{2}\gamma_{3D}. \tag{10}$$

Stewart, Siegel, and Goodstein[46] obtained a result consistent with Eq. (10) from a detailed study of vapor pressure of He^4 adsorbed on Grafoil. They used general thermodynamic relations to deduce chemical potentials and static compressibilities of the films, and using a 2D Debye model they deduced values for the longitudinal and transverse velocities of sound in the film. Their values for density $n=0.108$ Å^{-2} are $c_l=945$ m/s and $c_t=420$ m/s, indicating that the transverse modes in the film are the principal contributors to the heat capacity at low T.

The extreme sensitivity of heat capacity to coverage in the neighborhood of monolayer completion affords a sharper indication of completion than the conventional measurement by vapor pressure. Heat capacities can be measured at temperatures far below the range in which the vapor pressure is

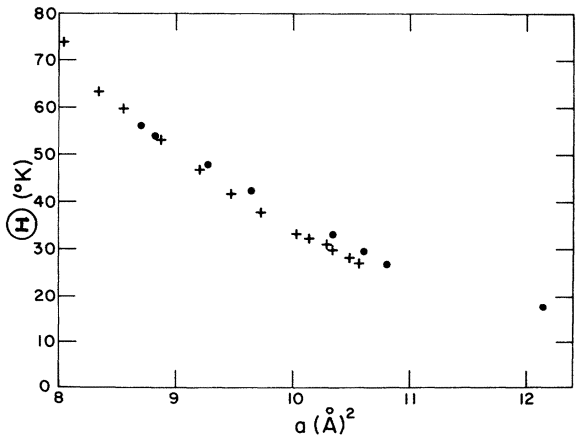

FIG. 24. Debye temperatures of He^4 monolayers (●) and hcp He^4 (+) on a common molecular-area scale.

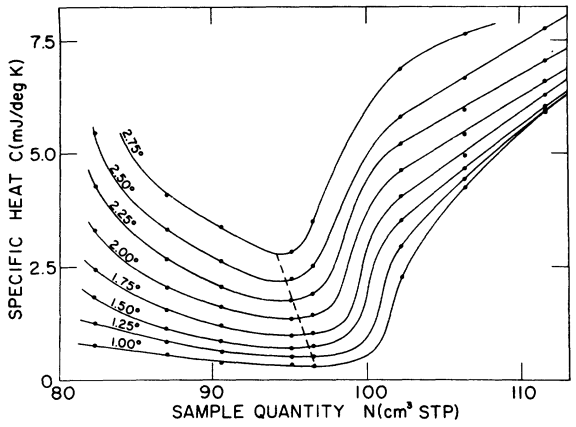

FIG. 25. Heat-capacity isotherms C vs N near monolayer completion. The points of monolayer completion are arbitrarily designated as the minima of the smooth curves.

detectable and therefore the thermal rounding of the steps in the isotherms can be reduced. Such a series of heat-capacity isotherms is shown in Fig. 25. We estimate from the isotherm at $T=1°K$ that full coverage of the first monolayer corresponds to density $n_1=0.115$ Å^{-2}. The values obtained from 4.2°K vapor-pressure isotherms (Table II) together with scaling from the $x_g=\frac{1}{3}$ values for He^4 in the two cells range from 0.115 to 0.119 Å^{-2}. A theoretical estimate by Campbell, Milford, Novaco, and Schick[100] is in close agreement with these values: Their calculated results are $0.1125\ \text{Å}^{-2}<n_1<0.1185\ \text{Å}^{-2}$ for a realistic range of repulsive-core atomic diameters. The energy-level difference between the first and second layers is extremely sensitive to sample quantity near first-layer completion: At completion the energy levels must coincide. If we attribute the temperature dependence of Θ for the highest coverage sample to second-layer excitation and analyze the results by a single-particle model the empirical energy-level difference between the two layers is found to be $(\epsilon_1-\epsilon_2)/k \simeq 11°K$; the second layer occupation at $T=1°K$ is then $N_2\simeq 1.7\times10^{-5}\,N$. Second-layer occupations at lower coverages are much smaller.

3. *"Melting" Anomalies*

At temperatures above the T^2 regions the heat capacities rise more steeply and develop pronounced maxima. As coverage is increased the anomalies progressively strengthen and shift to higher T, developing into spectacular peaks located above $T=7°K$ with heights greater than the

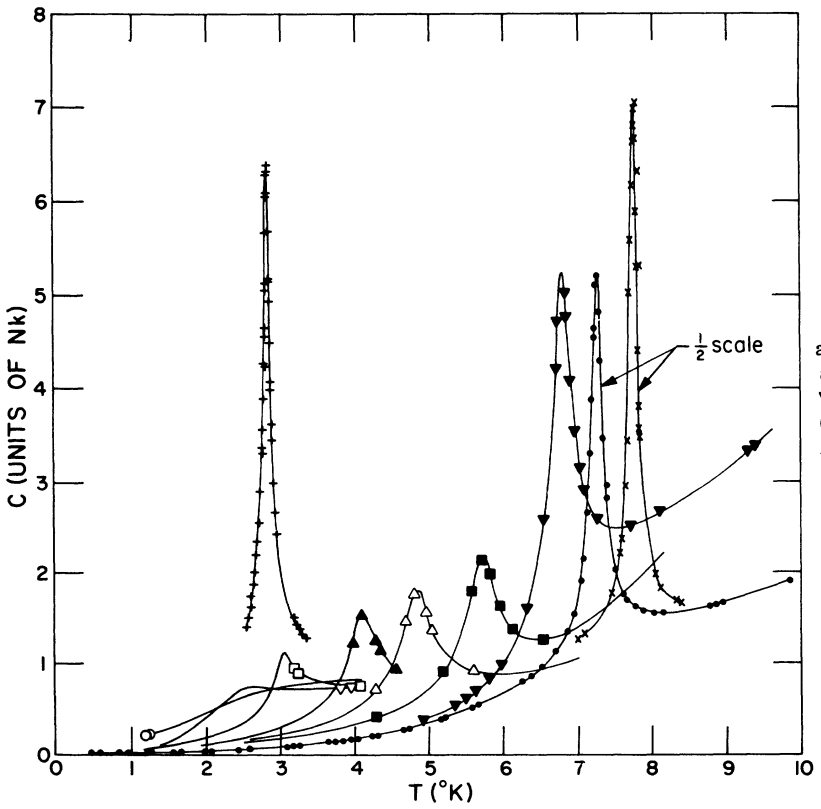

FIG. 26. High-density He^4 "melting" anomalies. Monolayer densities n Å^{-2} are +, 0.0637 ($x_g=1/3$); ○, 0.075; ▽, 0.0873; □, 0.0942; ▲, 0.0967; △, 0.0991; ■, 0.104; ▼, 0.108; ●, 0.115; ×, 0.133.

$x_g = \frac{1}{3}$ ordering peak (see Fig. 26). We believe that the high-density high-temperature peaks are associated with solid-fluid transformations.

Other mechanisms were considered, including lattice ordering, superfluidity, lateral condensation, and interlayer transitions. These alternatives were ruled out, for reasons outlined as follows. Lattice-gas ordering would imply exponential low-T specific heats in contrast to the observed T^2 dependences. Peak heights would be maximized at x_g values corresponding to simple fractions, whereas x_g ranges from 0.42 to 0.58 (after desorption corrections), with no reversal of trend at $x_g = \frac{1}{2}$. Furthermore, there are comparable peaks at similar densities in He^4 films on Xe-plated graphite, where the symmetry and spacing of sites are different.[101] Superfluidity was discarded after finding a strong high-temperature peak in a high-density He^3 film. Lateral condensation would require a very large lateral binding energy, much higher than theoretical estimates, and would imply phase coexistence at lower coverages and temperatures: this would be evidenced by a linear dependence on N at fixed T, $dc/dN = f(T)$,[11] contrary to the observations. Interlayer transitions are essentially single-particle processes, but the sharp peaks indicate collective behavior.

Quantitative comparison with melting temperatures of solid helium yields the strongest indication that the film peaks are associated with solid-liquid transformations. This is illustrated in Fig. 27, which presents the peak temperatures and the melting temperatures of hcp He^4[98] on a common-density scale. The correspondence between film and bulk is not as close as in the case of the Θ's, but is striking nevertheless. The two sets of data are nearly parallel, film values lying at 10–15% higher areas. The shift to lower density is consistent with the idea of steric hindrance of atoms constrained to a plane.

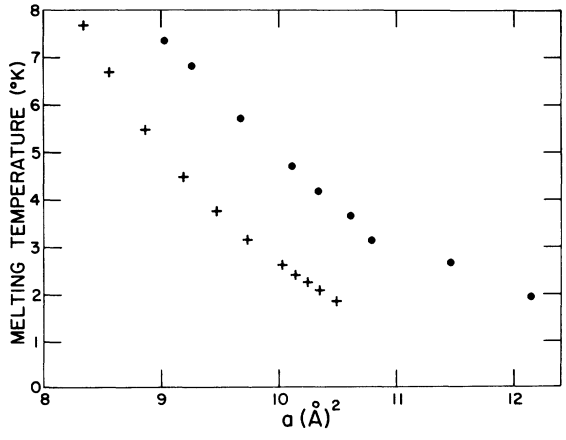

FIG. 27. Temperatures of the specific-heat anomalies in He^4 monolayers (●) and melting temperatures of hcp He^4 (+) on a common molecular-area scale.

If melting in the films were a first-order phase change, the heat capacities would be discontinuous at the boundaries of the two-phase regions, due to the abrupt appearance and disappearance of the transfer term $T(s_{\text{liq.}} - s_{\text{sol.}}) \times (dN/dT)_A$. On the contrary, the shapes of the anomalies, shown in Fig. 26, indicate that the solid-fluid transformation in the films is a continuous process. Continuous solid-liquid transformations in monolayers seem consistent with general theories[102,103] of the influence of dimensionality on crystalline order, which predict that long-range order cannot exist at finite temperatures in 2D systems. However, these theories do not prescribe a definite connection between the range of crystalline order and thermal effects due to melting. Dash and Bretz[104] have attempted to provide such a connection. They explored a number of 2D solid models and showed how the experimental anomalies might be directly related to the density of transverse-vibrational states. Their phenomenological theory leads to a possible explanation for the strong sharpening of the peaks at higher densities: It could be caused by the approach to a monolayer structure in partial registry with the substrate lattice. This registry would not have to be complete. As Ying has shown for classical arrays,[105] there can be "commensurate" structures of high order corresponding to rather large repeat distances. For any partially registered structures a film can have long-range order at finite T and therefore can melt by a first-order process. Indeed, a mechanism such as this has been invoked to explain the first-order melting of Ne monolayers on graphite.[106]

E. Very Low Densities

As density is decreased below $n \simeq 0.025$ Å^{-2} the heat capacities progressively change character from the gaslike behavior seen at higher densities and can no longer be understood in terms of weakly interacting models. The low-density region was explored primarily with He^4, but a single sample of low-density He^3 suggests that significant changes also occur in the lighter isotope. A more detailed study of low-density He^3 is now in progress.[94]

The observations are as follows. In the range 0.027 Å$^{-2} > n > 0.0036$ Å^{-2} the high-temperature ($T \sim 4$°K) specific heat increases monotonically with decreasing coverage from about k to twice this value, as can be seen in Table VII. The recent measurements by Elgin and Goodstein[83] are consistent with our results in that they also find large increases of specific heat above k at low cover-

ages. At the lowest density measured there appears to be a reversal of trend. For this sample the coverage amounted to 1.6% of a completed monolayer and the film contribution was only about 20% of the empty calorimeter, but the measured change in C/Nk from the next-higher-density film is well beyond the experimental scatter. For all but the lowest-density sample the specific heats have a sigmoid temperature dependence, with a moderately constant region near $T=4°K$, a steepest descent near 2°K, and decreasing slope at lower temperature. At the lowest density the region of steepest descent is at about 3.5°K and there is no definite tendency to level out at 4°K.

It is conceivable that at the lowest coverage we are observing effects of substrate heterogeneity. Grafoil must contain a finite fraction of graphite edge planes, whose binding energy is calculated[28] to be appreciably greater than basal-plane binding. Adsorption is preferential for strong-binding regions. If these consist of localizing sites or large long-range heterogeneities the low-temperature heat capacity will tend to lower values.

The characteristics at densities above the lowest are quite different and therefore cannot be explained simply on the basis of heterogeneity. (However, see *Note added in proof.*) Additional evidence for uniformity is seen in the behavior of the second atomic layer, i.e., films consisting of a low-density second layer on top of a completed first layer. As discussed in Sec. III D, in such samples the first layer continues to act as a high-density 2D solid with a characteristic temperature $\Theta \simeq 56°K$; therefore, the first-layer specific heat is quite low and does not obscure the contribution of a relatively small number of atoms in the second layer. In Sec. III D 3 we noted that a sample of He^4 at coverage $x=1.15$ was qualitatively different from one at $x=0.15$, in that no peak near $T=1°K$ was seen. We have also compared a sample at $x=1.05$ with one at $x=0.05$. In this case the second-layer contribution agrees with the low-density first layer. These results are illustrated in Fig. 28.

TABLE VII. Specific heat at $T \simeq 4$ °K of very-low-density films.

Isotope	Density n Å^{-2}	C/Nk
He^4	0.0273	0.934
	0.0164	1.05
	0.0158	1.05
	0.0122	1.18
	0.006 24	1.74
	0.003 64	2.14
	0.001 80	1.5 ±0.1
He^3	0.0415	0.862
	0.0154	1.03

The sigmoid temperature dependences and the nearly constant values $C=2\ Nk$ at high temperatures suggest 2D solid behavior, although a solid phase at such densities would seem impossible. Nevertheless, the similarity is striking: in Fig. 28 we show a theoretical 2D Debye specific heat fitted to the data, with characteristic temperature $\Theta=5.5°K$. The agreement leads us to call these films low-density solids and to so designate them in the phase diagram, but the name represents a convenience more than a conviction. It is of course possible that the adsorbed helium might interact by novel long-range forces due to substrate mediation and that these forces could cause the formation of a low-density solid phase. At the present time, however, this is only a speculation.

Note added in proof. Several experimental and theoretical results have come to our attention since the manuscript was submitted, and we feel that the following developments, as noted below, are particularly relevant to portions of this paper.

Siddon and Schick have extended their work on the quantum-mechanical virial coefficients of 2D gases.[56,57] Assuming a Lennard-Jones 6-12 interaction with the usual parameters for the 3D gas, i.e., $\epsilon/k=10.22°K$, $\sigma=2.56$ Å, they find for 2D He^4 that the calculated $B(T)$ provides close quantitative agreement with the specific heats of low-coverage films down to temperatures comparable to the specific-heat anomalies (somewhat below 2°K). We therefore believe that the high-temperature precursors of the He^4 anomalies are mainly

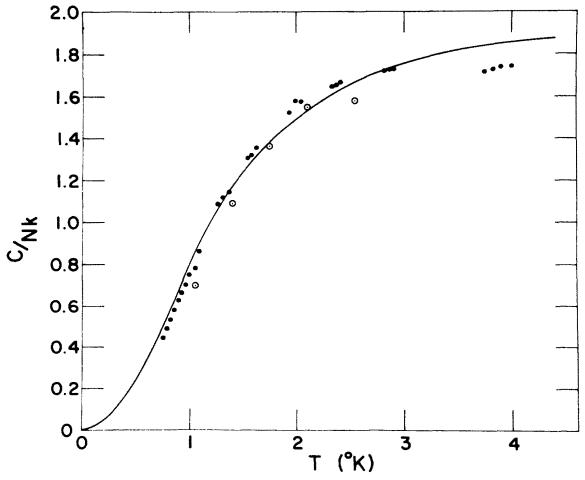

FIG. 28. Specific heat of He^4 at very low density. ●, fractional coverage $x=0.05$; density $n=0.00624$. ○, fractional coverage $x=1.05$, i.e., second-layer coverage $x_2=0.05$, after subtracting heat capacity of completed first layer. Solid line, 2D Debye theory, with $\Theta=5.5$ °K.

due to interactions and that lateral fields due to inhomogeneities of the substrate do not play important roles in this n, T range. The anomalies themselves appear to involve higher-order terms in a virial expansion. It is possible that the peaks are indicating some sort of lateral condensation to 2D liquid clusters, as Novaco[78] has suggested.

For He^3 Siddon and Schick find that the calculated $B(T)$ provides quantitative agreement with the specific heats down to about 0.5°K. An examination of the He^3 data, involving several different experimental samples at closely spaced coverages, shows that there is no significant contribution from higher-order virial coefficients down to this temperature even at relatively high densities, approaching those at which the lattice-gas ordering regime appears. From 0.5°K down to 0.2°K where the He^3 anomalies are found, contributions from higher-order virial terms begin to appear. However qualitative agreement with results calculated from $B(T)$ alone remains. Therefore we now abandon the spin-ordering hypothesis for the He^3 anomalies, and instead take it that they are caused by interactions.

Elgin and Goodstein[47,107] have combined their heat-capacity and vapor-pressure measurements to produce a highly detailed table of thermodynamic properties of He^4 on Grafoil. Their results are consistent with ours to within the accuracy of both sets of measurements. Elgin and Goodstein offer substantially different interpretations with respect to two regions of the phase diagram. They find that the isosteric heat of adsorption rises at very low coverages, indicating that a small fraction of the substrate area has appreciably greater binding energy, and they propose that this heterogeneity is responsible for the changes we observe in the heat capacity of He^4 as coverage is reduced below $x \simeq 0.1$ (see Sec. III E). In our discussion of that regime we mention heterogeneity as a possible cause and note that a degree of heterogeneity must be present due to a certain fraction of the area being composed of edge planes. Elgin and Goodstein have now obtained fairly convincing evidence of heterogeneity, although whether it is due to edge planes or, as they suggest, to wedge-shaped crevices where basal-plane surfaces join, cannot be determined from these measurements. They have also constructed a plausible model which allows them to calculate the heat capacity of films adsorbed on surfaces characterized by the measured variations in the heat of adsorption. The heterogeneities are assumed to be "homostattic,"[108] i.e., in the form of small homogeneous regions, distributed according to the empirical binding energy-area function. They take as a basis for the film characteristics a 2D van der Waals equation of state fitted to the high-temperature virial coefficients.[57] This model has no adjustable parameters, yet it yields calculated heat capacities in good quantitative agreement with the "low-density solid" results, at temperatures above 2°K. We feel that the direct evidence of heterogeneity from vapor pressure measurements and the success of this computational model are quite persuasive, even though a number of questions still need to be answered.

Elgin and Goodstein[47,107] have proposed an original explanation of the strong sharpening of the melting anomalies at high densities: that the enhancement is due to promotion of some atoms to a second layer as a result of a significant increase in the two-dimensional pressure upon melting. Combining our data on melting anomalies at lower coverages with their thermodynamic functions, they obtain extremely close fits to the shapes and heights of the enhanced peaks at high coverage. This calculation has a firmer and more quantitative basis than our speculation that the enhancement indicates the approach to registered phase at higher density.

The correspondence between the 2D solid phase of the film and bulk solid He^4 has been examined in much greater detail by Stewart.[109] He analyzed theoretical isotropic 2D and 3D elastic models including effects of initial stress due, in the 3D case, to external pressure P and, in films, to nonzero 2D spreading pressure ϕ. Stewart finds that the finite stress model works well for solid hcp He^4, yielding close agreement between Debye temperatures calculated from compressibility data and those determined from heat capacities. However, a consistent application of the same reasoning to 2D solid He, using compressibilities generated from the tables of Elgin and Goodstein,[47,107] does not yield comparable agreement with our values of the 2D Debye temperatures obtained from the film heat capacities. Thus, the virtual identity between the 2D and 3D Debye temperatures appearing in Fig. 24 seems to be accidental. There is a strong correspondence between the characteristic temperatures of films and bulk at equal values of the mean interatomic spacing, but in a more detailed comparison the similarity is not as close as we believed at first.

It now appears that the low coverage He^4 anomalies have not disappeared at equivalent second layer densities.[110] Rather, the peaks are suppressed a factor of 2 or 3 in temperature below the monolayer values. Although the physical mechanism for this suppression is not presently understood, we feel that these observations are consistent with the Siddon-Schick virial gas calculations.

ACKNOWLEDGMENTS

We are indebted to many people for important contributions to the experiments and interpretation. D. B. Fischbach suggested Grafoil as a substrate. Optical microscopy was made by P. M. Higgs and J. M. Tracy carried out x-ray diffraction analysis. S. Bukshpan supplied us with a chemical analysis. We benefited greatly from the related experiments of R. Rollefson and G. B. Huff, through the additional information gained from their results and from numerous conversations on monolayers in general. M. Schick and R. Siddon have been deeply involved in theoretical aspects of the project since its earliest stages, and for a portion of the period C. E. Campbell was also involved: Their contributions, through conversations, seminars, and working sessions have been extremely rewarding and productive. Several visitors contributed in important ways to our present understanding, including W. J. Mullin and M. Wortis. We are particularly grateful to R. E. Peierls, for his continuing advice and criticism over the course of the past several years. We thank D. L. Goodstein and R. L. Elgin for careful reading of the manuscript, for suggesting several improvements, and for correcting a number of errors.

---

*Research supported by the National Science Foundation.

†Present address: Physics Department, University of Michigan, Ann Arbor, Mich.

‡Present address: Cryogenic Center, Stevens Institute of Technology, Hoboken, N. J.

§Present address: Physics Department, University of California, Los Angeles, Calif.

[1]M. Bretz and J. G. Dash, Phys. Rev. Lett. **26**, 963 (1971).

[2]M. Bretz and J. G. Dash, Phys. Rev. Lett. **27**, 647 (1971).

[3]M. Bretz, G. B. Huff, and J. G. Dash, Phys. Rev. Lett. **28**, 729 (1972).

[4]D. C. Hickernell, E. O. McLean, and O. E. Vilches, Phys. Rev. Lett. **28**, 789 (1972).

[5]M. Bretz, Ph.D. thesis (University of Washington, 1971) (unpublished).

[6]E. O. McLean, Ph.D. thesis (University of Washington, 1972) (unpublished).

[7]H. P. R. Frederikse, Physica (Utr.) **15**, 860 (1949).

[8]D. F. Brewer, A. J. Symonds, and A. L. Thomson, Phys. Rev. Lett. **15**, 182 (1965); D. F. Brewer, A. Evenson, and A. L. Thomson, J. Low Temp. Phys. **3**, 603 (1970).

[9]For a review of monolayer and multilayer measurements of helium films on Vycor glass substrates, see D. F. Brewer, J. Low Temp. Phys. 3, 205 (1970).

[10]D. L. Goodstein, J. G. Dash, and W. D. McCormick, Phys. Rev. Lett. **15**, 447 (1965); W. D. McCormick, D. L. Goodstein, and J. G. Dash, Phys. Rev. **168**, 249 (1968).

[11]G. A. Stewart and J. G. Dash, Phys. Rev. A **2**, 918 (1970).

[12]R. H. Anderson and T. C. Foster, Phys. Rev. **151**, 190 (1966).

[13]C. E. Campbell and M. Schick, Phys. Rev. A **3**, 691 (1971).

[14]M. D. Miller, C. W. Woo, and C. E. Campbell, Phys. Rev. A **6**, 1942 (1972).

[15]M. Schick and C. E. Campbell, Phys. Rev. A **2**, 1591 (1970).

[16]G. A. Stewart and J. G. Dash, J. Low Temp. Phys. **5**, 1 (1971).

[17]D. W. Princehouse, J. Low Temp. Phys. **8**, 287 (1972).

[18]P. Mahadev, M. F. Panczyk, R. A. Scribner, and J. G. Daunt, Phys. Lett. A **41**, 221 (1972).

[19]J. G. Daunt, Phys. Lett. A **41**, 223 (1972).

[20]N. N. Roy and G. D. Halsey, Jr., J. Low Temp. Phys. **4**, 231 (1971).

[21]D. M. Young and R. D. Crowell, *Physical Adsorption of Gases* (Butterworths, London, England, 1962).

[22]M. H. Polley, W. D. Schaeffer, and W. R. Smith, J. Phys. Chem. **57**, 469 (1953); W. D. Schaeffer, W. R. Smith, and M. H. Polley, Ind. Eng. Chem. **45**, 172 (1953).

[23]R. H. Fowler and E. A. Guggenheim, *Statistical Thermodynamics* (Cambridge U.P., Cambridge, England, 1939), pp. 426–444.

[24]T. L. Hill, J. Chem. Phys. **15**, 767 (1947).

[25]G. D. Halsey, Jr., J. Am. Chem. Soc. **73**, 2693 (1951); J. Am. Chem. Soc. **74**, 1082 (1952).

[26]R. E. Franklin, Acta Crystallogr. **4**, 253 (1951).

[27]L. L. Ban and W. M. Hess, in Proceedings of the Ninth Biennial Conference on Carbon, Boston 1969 (unpublished).

[28]R. M. Barrer, Proc. R. Soc. A **161**, 476 (1937).

[29]G. Ehrlich and F. G. Hudda, J. Chem. Phys. **30**, 493 (1959).

[30]T. Engel and R. Gomer, J. Chem. Phys. **52**, 5572 (1970).

[31]J. H. Singleton and G. D. Halsey, Jr., J. Phys. Chem. **58**, 1011 (1954).

[32]For a recent discussion of BET theory and applications, see S. Brunauer, L. E. Copeland, and D. L. Kantro, *The Solid Gas Interface*, edited by E. A. Flood (Marcel Dekker, New York, 1967), Vol. I., Chap. 3.

[33]A. R. Ubbelhode and F. A. Lewis, *Graphite and its Compounds* (Oxford U.P., Oxford, England, 1960).

[34]X. Duval and A. Thomy, C.R. Acad. Sci. (Paris) **259**, 4007 (1964).

[35]A. Thomy and X. Duval, J. Chim. Phys. **66**, 1966 (1969); J. Chim. Phys. **67**, 286 (1970); J. Chim. Phys. **67**, 1101 (1970).

[36]Grafoil is the trademark of a product marketed by Union Carbide Carbon Products Division, 270 Park Avenue, New York, N. Y.

[37]D. B. Fischbach (private communication).

[38]S. Bukshpan, Israel Atomic Energy Commission, Soreq Research Center, Yavne, Israel (private communication).

[39]J. M. Tracy (private communication).

[40]P. M. Higgs (private communication).

[41]CryoCal, Inc., 1371 Avenue E., Riviera Beach, Calif., model No. CR-250.

[42]S.H.E. Mfg. Co., La Jolla, Calif.

[43]MKS Instruments, Inc., Burlington, Mass.

[44]G. T. McConville, Cryogenics **9**, 122 (1969).

[45]J. G. Daunt and E. Lerner, J. Low Temp. Phys. **10**, 299 (1973).

[46]G. A. Stewart, S. Siegel, and D. L. Goodstein, in Proceedings of the Thirteenth International Conference on Low Temperature Physics, Boulder, Colo. 1972 (unpublished).

[47]R. L. Elgin and D. L. Goodstein, in Ref. 46; Proceedings of the Symposium on Monolayer and Submonolayer Helium Films, Stevens Insitute of Technology, 1973 (unpublished).

[48]All of our results are summarized and discussed in this paper but only a small representative portion of the total number of

data points can be explicitly tabulated or shown in graphs. In all we made measurements on 99 samples in experimental systems A or B: There were usually over 30 individual specific-heat determinations on each sample. We attempt to present in this paper a comprehensive digest and analysis of the measurements. However we realize that some readers may wish to examine the data in detail in order to test specific models or to compare our results with subsequent measurements. Therefore, we will make available a limited number of copies of the complete data in tabular form. Requests for data sets of specific heats of He^3 and He^4 monolayer films on graphite should be addressed to the Low-Temperature Laboratory, Physics Department, University of Washington, and should refer to this paper.

[49]D. E. Hagen, A. D. Novaco, and F. J. Milford, in *Proceedings of the Second International Conference on Adsorption-Desorption Phenomena, Florence, Italy 1971* (Academic, New York, 1972).

[50]J. G. Dash and M. Bretz, Phys. Rev. **174**, 247 (1968).

[51]F. J. Milford and A. D. Novaco, Phys. Rev. A **4**, 1136 (1971).

[52]L. Landau and E. M. Lifshitz, *Statistical Physics* (Pergamon, London, England, 1958), Chap. 7.

[53]T. L. Hill, J. Chem. Phys. **14**, 441 (1946).

[54]W. A. Steele, *The Solid-Gas Interface*, edited by E. A. Flood (Marcel Dekker, New York, 1967), Vol. I., Chap. 10.

[55]L. J. Slutsky and G. D. Halsey, in *Physical Chemistry*, edited by H. Eyring (Academic, N. Y. 1967), Vol. 2, Chap. 9.

[56]R. L. Siddon and M. Schick, in Proceedings of the Symposium on Monolayer and Submonolayer Helium Films, Stevens Institute of Technology, 1973 (unpublished).

[57]R. L. Siddon, PhD. thesis (University of Washington, 1973) (unpublished).

[58]R. M. May, Phys. Rev. **135**, A1515 (1964).

[59]W. E. Keller, *Helium-3 and Helium-4* (Plenum, New York, 1969).

[60]M. F. Panczyk, R. A. Scribner, G. C. Straty, and E. D. Adams, Phys. Rev. Lett. **19**, 1102 (1967).

[61]J. R. Sites, D. D. Osheroff, R. C. Richardson, and D. M. Lee, Phys. Rev. Lett. **23**, 835 (1969).

[62]R. T. Johnson, O. G. Symko, and J. C. Wheatley, Phys. Rev. Lett. **23**, 1017 (1969).

[63]H. M. Guo, D. O. Edwards, R. E. Sarwinski, and J. T. Tough, Phys. Rev. Lett. **27**, 1259 (1971).

[64]A. F. Andreev, Zh. Eksp. Teor. Fiz. **50**, 1415 (1966) [Sov. Phys.-JETP **23**, 939 (1966)].

[65]L. Goldstein, Phys. Rev. **96**, 1455 (1954).

[66]For a discussion of Goldstein's theory with comparisons to experiments, see Ref. 59, pp. 78–190.

[67]P. C. Hohenberg, Phys. Rev. **158**, 383 (1967).

[68]M. F. M. Osborne, Phys. Rev. **76**, 396 (1949).

[69]J. M. Ziman, Philos. Mag. **44**, 548 (1953).

[70]D. L. Mills, Phys. Rev. **134**, A306 (1964).

[71]D. F. Goble and L. E. H. Trainor, Can. J. Phys. **44**, 27 (1965).

[72]D. Krueger, Phys. Rev. **172**, 211 (1968).

[73]Y. Imry, Ann. Phys. (N.Y.) **51**, 1 (1969).

[74]D. Jasnow and M. E. Fisher, Phys. Rev. B **3**, 895 (1971).

[75]M. Barber and M. E. Fisher (unpublished).

[76]C. E. Campbell, J. G. Dash, and M. Schick, Phys. Rev. Lett. **26**, 966 (1971).

[77]A. Widom and J. B. Sokoloff, Phys. Rev. A **5**, 475 (1972).

[78]A. D. Novaco, J. Low Temp. Phys. **9**, 457 (1972).

[79]O. Sinanoğlu and K. S. Pitzer, J. Chem. Phys. **32**, 1279 (1960).

[80]G. B. Huff, Ph.D. thesis (University of Washington, 1972) (unpublished).

[81]J. J. Lander and J. A. Morrison, Surf. Sci. **6**, 1 (1967).

[82]Y. Baskin and L. Meyer, Phys. Rev. **100**, 544 (1955).

[83]Reference 47.

[84]R. J. Rollefson, Phys. Rev. Lett. **29**, 410 (1972).

[85]R. H. Fowler, Proc. Camb. Philos. Soc. **32**, 144 (1936).

[86]R. E. Peierls, Proc. Camb. Philos. Soc. **32**, 477 (1936).

[87]L. Onsager, Phys. Rev. **65**, 117 (1944).

[88]G. F. Newell and E. W. Montroll, Rev. Mod. Phys. **25**, 353 (1953).

[89]C. Domb, Adv. Phys. **9**, 149 (1960); Adv. Phys. **9**, 245 (1960).

[90]M. E. Fisher, Rep. Prog. Phys. **30**, 615 (1967).

[91]T. D. Lee and C. N. Yang, Phys. Rev. **87**, 810 (1952).

[92]C. E. Campbell and M. Schick, Phys. Rev. A **5**, 1919 (1972).

[93]N. F. Mott, Rev. Mod. Phys. **40**, 677 (1968).

[94]A. E. Ferdinand and M. E. Fisher, Phys. Rev. **185**, 832 (1969).

[95]B. M. McCoy and T. T. Wu, Phys. Rev. **176**, 631 (1968).

[96]M. Schick and R. L. Siddon, Phys. Rev. A **8**, 339 (1973).

[97]S. V. Hering and O. E. Vilches, in Ref. 56.

[98]G. Ahlers, Phys. Rev. A **2**, 1505 (1970).

[99]J. G. Dash, J. Low Temp. Phys. **1**, 173 (1969).

[100]C. E. Campbell, F. J. Milford, A. D. Novaco, and M. Schick, Phys. Rev. A **6**, 1648 (1972).

[101]G. B. Huff (private communication).

[102]R. E. Peierls, Ann. Inst. Henri Poincare **5**, 177 (1935).

[103]N. D. Mermin, Phys. Rev. **176**, 250 (1968).

[104]J. G. Dash and M. Bretz, J. Low Temp. Phys. **9**, 291 (1972).

[105]S. C. Ying, Phys. Rev. B **3**, 4160 (1971).

[106]G. B. Huff and J. G. Dash, in Ref. 46.

[107]R. L. Elgin, Ph.D. thesis (California Institute of Technology, 1973) (unpublished).

[108]S. Ross and J. P. Olivier, *On Physical Adsorption* (Interscience, New York, 1964).

[109]G. A. Stewart (unpublished).

[110]M. Bretz, in Ref. 56.